ISSN 2744-2640
e-ISSN 2744-2659
JST&M, Vol. 4
www.fipn.unze.ba
06

Journal of **Sustainable Technologies and Materials**

Zenica, Juni 2024

Journal of Sustainable Technologies and Materials (ISSN 2744-2640)
Vol. 4, No. 6(2023), 1 – 34

Published by
The University of Zenica, Faculty of Engineering and Natural Sciences

Editorial office
Travnička cesta 1,72000 Zenica
Bosnia and Herzegovina
Phone: +387 32 403 468
Email: jstm@unze.ba
Website: https://www.fipn.unze.ba

Editor-in-Chief
Farzet Bikić, The University of Zenica, Faculty of Engineering and Natural Sciences, B&H

Associate Editors
Hasan Avdušinović, B&H, University of Zenica, Faculty of Engineering and Natural Sciences
Ilhan Bušatlić, B&H, University of Zenica, Faculty of Engineering and Natural Sciences
Diana Ćubela, B&H, University of Zenica, Faculty of Engineering and Natural Sciences
Jusuf Duraković, B&H, University of Zenica, Faculty of Engineering and Natural Sciences
Almaida Gigović-Gekić, B&H, University of Zenica, Faculty of Engineering and Natural Sciences
Adnan Mujkanović, B&H, University of Zenica, Faculty of Engineering and Natural Sciences
Editorial Board Members
Elvis Ahmetović, B&H, University of Tuzla, Faculty of Technology,
Ljubiša Balanović, Serbia, University of Belgrade, Technical Faculty Bor,
Mirjana Čurlin, Croatia, University of Zagreb, Faculty of Food Technology and Biotechnology
Sead Ćatić, B&H, University of Tuzla, Faculty of Technology
Kemal Delijić, Montenegro, University of Montenegro, Faculty of Metallurgy and Technology,
Natalija Dolić, Croatia, University of Zagreb, Faculty of Metallurgy Sisak,
Mirko Gojić, Croatia, University of Zagreb, Faculty of Metallurgy Sisak,
Nenad Gubeljak, Slovenia,
The University of Maribor, Faculty of Mechanical Engineering,
Safija Herenda, B&H, University of Sarajevo, Faculty of Science
Nusret Imamović, B&H, University of Zenica, Faculty of Mechanical Engineering
Fehim Korać, B&H, University of Sarajevo, Faculty of Sciences
Borut Kosec, Slovenia, University of Ljubljana, Faculty of Natural Sciences and Engineering
Tibela Landeka Dragičević, Croatia, University of Zagreb, Faculty of Food Technology and Biotechnology
Dragan Manasijević, Serbia, University of Belgrade, Technical Faculty Bor
Sanja Martinović, Serbia, University of Belgrade, Faculty of Technology and Metallurgy
Viorica Musat, Romania, "Dunărea de Jos" University of Galati, **Aleš Nagode**, Slovenia, University of Ljubljana, Faculty of Natural Sciences and Engineering.
Vesna Ocelić Bulatović, Croatia, University of Zagreb, Faculty of Metallurgy Sisak
Iulian Riposan, Romania, University Politehnica of Bucharest, Materials Science and Engineering Faculty
Luca Sportelli, New Zealand, St. Clements University, Niue,
Aida Šapčanin, B&H, University of Sarajevo, Faculty of Pharmacy
Nada Štrbac, Serbia, University of Belgrade, Technical Faculty Bor
Anita Štrkalj, Croatia, University of Zagreb, Faculty of Metallurgy Sisak,
Iveta Vaskova, Slovakia, Technical University of Košice, Faculty of Materials, Metallurgy and Recycling,
Asim Vehbi, North Cyprus,
Arkin University of Creative Arts and Design (ARUCAD)
Milica Vlahović, Serbia, University of Belgrade, Faculty of Technology and Metallurgy,
Tatjana Volkov-Husović, Serbia, University of Belgrade, Faculty of Technology and Metallurgy,
Zdenka Zovko Brodarac, Croatia, University of Zagreb, Faculty of Metallurgy Sisak,

English Language Editor
Hasan Avdušinović, University of Zenica, Faculty of Engineering and Natural Sciences, B&H
Diana Ćubela, University of Zenica, Faculty of Engineering and Natural Sciences, B&H

For submission instructions, manuscript submission, and additional information, please visit https://www.fipn.unze.ba/.

Disclaimer: The Publisher and Editors cannot be held responsible for errors or any consequences arising from the use of the information contained in this journal. The views and opinions expressed do not necessarily reflect those of the Publisher and Editors, and neither does the publication of advertisements constitute any endorsement by the Publisher and Editors of the product advertised.

Computer design
Safet Hamedović, University of Zenica, Faculty of Engineering and Natural Sciences

Cover design:
Admir Velić

Printed by „Štamparija Fojnica" D.D. Fojnica, B&H, in June 2024

Journal of Sustainable Technologies and Materials

JSTM

CONTENTS

JST&M 6(2024), 1 - 7
DOI: 10.57131/jstm.2024.6.1

Original scientific paper

CHARGE CARRIERS STATES IN A MODEL OF CuO SUPERCONDUCTIVE CERAMICS

Jovan P. Šetrajčić[1], Siniša M. Vučenović[2]

[1]Academy of Sciences and Arts of the Republic of Srpska
[2]University of Banja Luka, Faculty of Sciences and Mathematics

ABSTRACT

The translational symmetry of the distribution of atoms (ions) of the charge carriers (electrons or holes) system is broken by sputtering (doping) due to the existence of two boundary surfaces. This is a model of high-temperature superconductors in which the observed symmetry breaking orthogonal to the CuO plane is treated as a perturbation. Single-particle fermion wave functions and possible charge carrier energies were determined. The competing existence of superconducting and normal regions in such a sample is shown in agreement with experimental data. The conditions for the formation of superconducting states and the limits of the current density values in the planes parallel to the boundary surfaces (in the CuO planes) were obtained and discussed.

Keywords: ceramic oxides, charge carriers, dispersion law, energy states

Corresponding Author:
Siniša M. Vučenović
University of Banja Luka, Faculty of Sciences and Mathematics
Mladena Stojanovića 2, 78000 Banja Luka
Tel: ++ 387 51 315 694
E-mail address: sinisa.vucenovic@pmf.unibl.org

1. INTRODUCTION

High-temperature superconducting ceramics have "broken" the myth of an exclusively low-temperature effect of superconductivity [1–4]. Although they were discovered and improved at the end of the last century, the mechanism of superconductivity has not been figured out to date. The biggest difficulty is their highly anisotropic structure (Figure 1).

The answer to the question of the oxide ceramics superconductivity mechanism must be undoubtedly sought in the phonon subsystem, in the elementary charges subsystem as well as in the interaction of these subsystems. Concerning the very anisotropic structure of the superconductive ceramics [1,2], we have attempted to construct a theoretical model conveying the broken translational symmetry of atoms (molecules) arrangement along one direction in the crystal lattice, the difference in masses of these molecules, and the presence of two boundary planes along this direction [5,6].

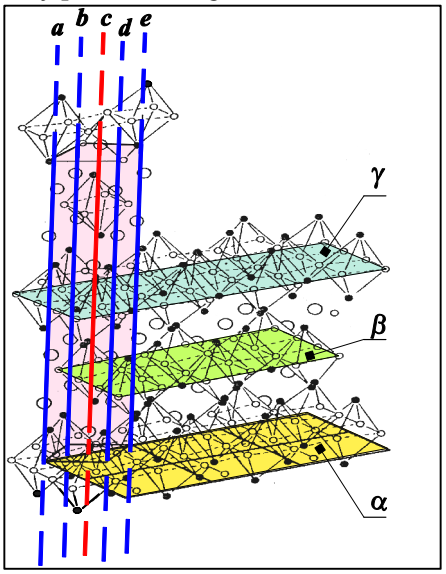

Figure 1. Model of high-temperature superconductors – CuO ceramics

The phonon system is drawn out in this model [6]. We have determined the phonon states and their energy spectra and have shown that, due to the broken crystal symmetry (actually because of deformed and tiny granular structure), the phonons of optical type owning the energy gap are present here [7]. The next task we have attempted to solve is to determine and analyse the spectra of free charge carriers (electrons or holes), the Landau criterion, and the probabilities of states and entropy within the same model. The preliminary results are already presented [8,9].

2. MODEL HAMILTONIAN

To obtain the Hamiltonian of the charge carriers in the structure with broken translational symmetry, it is most suitable to start with the standard Hamiltonian of the electron system in an ideal infinite structure [10–12]:

$$H_{id} = \sum_{\vec{k}} \frac{\hbar^2\vec{k}^2}{2m^*}\, C_{\vec{k}}^{+} C_{\vec{k}}, \qquad (1)$$

where m^* is electron effective mass, while $C_{\vec{k}}^{+}$ and $C_{\vec{k}}$ are Fermi creation and annihilation operators of electrons with momentum $\hbar\vec{k}$ and energy $\hbar^2\vec{k}^2(2m^*)^{-1}$. If we go over to the configuration space using the transformations:

$$C_{\vec{k}} = \frac{1}{\sqrt{N}}\sum_{\vec{n}} C_{\vec{n}} \mathrm{e}^{-i\vec{k}\vec{n}}; \qquad C_{\vec{k}}^{+} = \frac{1}{\sqrt{N}}\sum_{\vec{n}} C_{\vec{n}}^{+} \mathrm{e}^{i\vec{k}\vec{n}}, \quad (2)$$

where N is the number of molecules in the considered structure, we get:

$$H_{id} = \sum_{\vec{n}} \Lambda C_{\vec{n}}^{+} C_{\vec{n}} - \sum_{\vec{n},\vec{m}} W_{\vec{n}\vec{m}} C_{\vec{n}}^{+} C_{\vec{m}}. \qquad (3)$$

Here $\Lambda = N^{-1}\sum_{\vec{k}} \frac{\hbar^2\vec{k}^2}{2m^*}$ and $W_{\vec{n}\vec{m}} = -N^{-1}\sum_{\vec{k}} \frac{\hbar^2\vec{k}^2}{2m^*}\, \mathrm{e}^{i\vec{k}(\vec{n}-\vec{m})}$. Due to the canonicity of the transformation (2), the operators $C_{\vec{n}}^{+}$ and $C_{\vec{n}}$ are also Fermi operators.

Let us recall the most important assumptions of our model: we consider the tetragonal i.e. generalized cubic structure with very high anisotropy along the z-axis. It means that the lattice constant in this direction (a_z) is a few times larger than the lattice constant a_x, a_y in the directions x and y. The translational symmetry is fully conserved in the XY planes, while the symmetry of the masses arrangement along the z direction is broken (during the doping of the ceramic structure by the introduction of foreign atoms, the sputtered atoms located along this direction because it is energetically most convenient). We also assume here that the structure under consideration is a film (not necessarily thin!). It means that the components of lattice vector $\vec{n} \equiv (n_x, n_y, n_z)$ vary in the following way:

$$n_r \in \left(-\frac{N_r}{2}, +\frac{N_r}{2}\right), \; r = (x,y); \;\; n_z \in [0, N_z] \qquad (4)$$

The numbers of atoms N_x and N_y along the directions x and y, respectively, may be indefinitely high since we have the translational symmetry along these directions. The number of atoms along z direction (N_z) is limited. The above-described model, i.e. the highly anisotropic matrix along the z direction, necessarily doped with foreign atoms, can be used for getting some qualitative conclusions about the superconductive ceramics behaviour. It is known [1–3] that the ceramic oxides are anisotropic along one privileged direction and that the superconductive state is realised by doping. But the real structure of the ceramic oxides–perovskites is approximated by the tetragonal structure. It is also assumed in the model that the sputtering is symmetric on both boundary planes: $n_z = 0$ and $n_z = N_z$ and between the layers $n_z = 0$ and $n_z = 1$ (as well as between the layers $n_z = N_z - 1$ and $n_z = N_z$) n_0 foreign particles are placed, in such a way that the structure of the doped matrix is unchanged near the middle of the film.

If the behaviour of the quantities from (3) may be expressed by the law:

$$W_{\vec{n}\vec{m}} = \frac{W_0}{|\vec{n}-\vec{m}|^h}; \qquad W_0 > 0; \qquad h > 0, \qquad (5)$$

in the nearest neighbors approximation, we get:

$$W_{n_s;n_s\pm1} \equiv W_s = W_0\, a_s^{-h}; \qquad s = (x,y,z). \qquad (6)$$

According to the described view of the doping, it is obvious that lattice constant a_z in the doped structure becomes dependent on the position n_z, i.e. $a_z \longrightarrow a_z(n_z)$. Because of the symmetry on the boundaries: $a_z(0) = a_z(N_z) = a_z(n_0+1)^{-1}$; $a_z(N_z/2) = a_z$, we may take:

$$a_z(n_z) = a_z\left(1 - \frac{n_0}{n_0+1}\, N_z^2\right); \; N_z^2 = 2n_z N_z^{-1} - 1. \qquad (7)$$

The dependence of the lattice constant on the index n_z causes the dependence of the interaction along z direction on the index n_z, i.e.:

$$W_z \longrightarrow W_z(n_z) = W_0 a_z^{-h}(n_z) = W_0 a_z^{-h}\left(1 - N_z^2 \frac{n_0}{n_0+1}\right)^{-h} \approx W_z(1 + \Phi N_z^2), \tag{8}$$

where $\Phi = hn_0(n_0+1)^{-1}$. The interactions W_x and W_y, according to the described picture, are unchanged. We must notice that the last two expressions are valid for even N_z. But, for large enough N_z ($N_z \approx N_z + 1$), or during the transition from n_z to continual variable z, the deviations from the formulas (7) and (8) for odd N_z are not essential. The values of Λ are not dependent on the index of the site, because of they are unchanged during the doping. Hence we can write the Hamiltonian of the doped structure in the form:

$$H = H_{\mathrm{B}} + H_{\mathrm{V}}, \tag{9}$$

where:

$$\begin{aligned} H_{\mathrm{B}} = \sum_{n_x,n_y} \Big\{ & C^+_{n_x n_y 0}\Big[\Lambda C_{n_x n_y 0} - W_x\left(C_{n_x+1,n_y 0} + C_{n_x-1,n_y 0}\right) - \\ & - W_y\left(C_{n_x n_y+1,0} + C_{n_x n_y-1,0}\right) - W_z(1-\Phi)C_{n_x n_y 1}\Big] + \\ & + C^+_{n_x n_y N_z}\Big[\Lambda C_{n_x n_y N_z} - W_x\left(C_{n_x+1,n_y N_z} + C_{n_x-1,n_y N_z}\right) - \\ & - W_y\left(C_{n_x n_y+1,N_z} + C_{n_x n_y-1,N_z}\right) - W_z(1-\Phi)C_{n_x n_y N_z-1}\Big]\Big\}, \end{aligned} \tag{10}$$

and, as we can see, it is related to the boundary layers ($n_z = 0$ and $n_z = N_z$), where $W_{n_x,n_y,0;n_x,n_y,-1} = W_{n_x,n_y,N_z;n_x,n_y,N_z+1} = 0$, and for H_{V} we find:

$$\begin{aligned} H_{\mathrm{V}} = \sum_{n_x,n_y} \sum_{n_z=0}^{N_z-1} \Big\{ & C^+_{n_x n_y 0}\Big[\Lambda C_{n_x n_y 0} - W_x\left(C_{n_x+1,n_y 0} + C_{n_x-1,n_y 0}\right) - \\ & - W_y\left(C_{n_x n_y+1,0} + C_{n_x n_y-1,0}\right) - W_z(1-\Phi)C_{n_x n_y 1}\Big] + \\ & + C^+_{n_x n_y N_z}\Big[\Lambda C_{n_x n_y N_z} - W_x\left(C_{n_x+1,n_y N_z} + C_{n_x-1,n_y N_z}\right) - \\ & - W_y\left(C_{n_x n_y+1,N_z} + C_{n_x n_y-1,N_z}\right) - W_z(1-\Phi)C_{n_x n_y N_z-1}\Big]\Big\}. \end{aligned} \tag{11}$$

3. SINGLE-PARTICLE STATES OF THE SYSTEM

We shall analyse the system described by Hamiltonian (9) using the orthonormalized single-electron state functions [12]:

$$|\Psi\rangle = \sum_{n_x,n_y,n_z} A_{n_x,n_y,n_z} C^+_{n_x,n_y,n_z}|0\rangle; \qquad \sum_{n_x,n_y,n_z} |A_{n_x,n_y,n_z}|^2 = 1. \tag{12}$$

We obtain the equations for finding the coefficient A_{n_x,n_y,n_z} using the equations of motion for operators C_{n_x,n_y,n_z}. From $C_{n_x,n_y,n_z}(t) = C_{n_x,n_y,n_z}(0)e^{i\omega t}$, $\omega = E/\hbar$, it follows:

$$E\, C_{n_x,n_y,n_z} - \left[C_{n_x,n_y,n_z}, H\right] \equiv O_{n_x,n_y,n_z}; \qquad O_{n_x,n_y,n_z} = O. \tag{13}$$

Based on equations (9 –11) and (13), we form operators $O_{n_x,n_y,0}$, O_{n_x,n_y,N_z} and O_{n_x,n_y,n_z}. After applying them to the functions (12) and using the substitution:

$$A_{n_x,n_y,n_z} = A_{n_z} e^{i(n_x a_x k_x + n_y a_y k_y)}, \tag{14}$$

where $k_j = \frac{2\pi}{N_j a_j}\nu_j$; $j = (x,y)$; $\nu_j \in \left(-\frac{N_j}{2}, +\frac{N_j}{2}\right)$ and based on the fact that $\Lambda = 2\sum_{xyz} W_j$, we find the following system of difference equations:

$$(E - 4Q - 2W_z)A_0 + W_z(1-\Phi)A_1 = 0, \qquad n_z = 0;$$

$$(E - 4Q - 2W_z)A_{N_z} + W_z(1-\Phi)A_{N_z-1} = 0, \qquad n_z = N_z; \tag{15}$$

$$(E - 4Q - 2W_z)A_{n_z} + W_z(1+\Phi N_z^2)\left(A_{n_z+1} + A_{n_z-1}\right) = 0, \quad 1 \le n_z \le N_z - 1, \tag{16}$$

where $Q \equiv Q_{k_x k_y} = W_x \sin^2\left(\frac{a_x k_x}{2}\right) + W_y \sin^2\left(\frac{a_y k_y}{2}\right)$. We shall perform further analysis in the continual approximation to avoid the complications arising during the determination of the coefficient A_n from the system of difference equations (15). Introduction of the continual variable z through $n_z \to z/a_z$ ($N_z \to L/a_z$) causes the following transformations of the expressions (7) and (8):

$$a_{z;n_z} \to a_z(z) = a_z\left[1 - \frac{n_o}{n_o+1}\left(2\frac{z}{L} - 1\right)^2\right], \quad W_{z;n_z} \to W_z(z) = W_z\left[1 + \Phi\left(2\frac{z}{L} - 1\right)^2\right]. \tag{17}$$

The coefficients A_{n_z} will be transformed in the following way:

$$A_n \to A(z)\ ; \qquad A_{n+1} + A_{n-1} \to A(z + \bar{a}_z) + A(z - \bar{a}_z), * 1.0mm$$

$$A(z \pm \bar{a}_z) \approx A(z) \pm \bar{a}_z \frac{dA}{dz} + \frac{\bar{a}_z^2}{2}\frac{d^2A}{dz^2}; \qquad \bar{a}_z \equiv \bar{a}_z(z) = \frac{1}{L}\int_0^L dz a_z(z) = a_z \frac{2n_o+3}{3(n_o+1)}.$$

The important consequence of the transition to the continuum is the fact that the first two equations from (15) vanish from the calculation at $n_z \to z$, i.e. they are merged into the last of equations from (15), which is the continual approximation has the form:

$$\frac{d^2A}{dz^2} + \frac{E-4Q-\Phi(E-4Q-2W_z)\left(2\frac{z}{L}-1\right)^2}{\bar{a}_z^2(z)\,W_z} A = 0. \qquad (18)$$

By the assumption:

$$E > 4Q + 2W_z \equiv E_z^{(0)} \qquad (19)$$

and by the substitution: $2z/L - 1 = \tau\zeta$, with $\tau^4 = W_z(\bar{a}_z L)^2\,[4\Phi\,(E-4Q-2W_z)]^{-1}$, the equation (17) becomes known Hermite-Weber equation:

$$\frac{d^2A}{d\zeta^2} + (\kappa - \zeta^2)A = 0, \qquad (20)$$

where $\kappa = \frac{L}{2\bar{a}_z}(E-4Q)\left[\Phi\,(E-E_z^{(0)})W_z\right]^{-1/2}$.

Here we introduce the requirement that the amplitudes A are finite for arbitrary structure thickness (it means even for $L \to \infty$ too). To satisfy this requirement we must take the known condition of the finiteness for the solutions for the Hermite-Weber equation: $\kappa = 2\mu + 1; \quad \mu = 0,1,2,\ldots$ Based on this we find:

$$E_{1,2} = 4Q + 2b^2(2\mu+1)^2\Phi W_z\left\{1 \pm \left[1 - \frac{2}{(2\mu+1)^2 b^2 \Phi}\right]^{1/2}\right\}, \qquad (21)$$

were $b = \bar{a}_z/L$. The expression for energies (20) indicates that index μ must be limited from below (the energies must be real):

$$2\,\mu \;\geq\; b^{-1}\sqrt{2/\Phi} - 1. \qquad (22)$$

It means that the minimal allowed value of the index μ is the minimal integer which is bigger than the final term in (20). As we can see, the lower boundary of quantum number μ depends on the number of structural layers (through N_z), on the way of sputtering (through n_0), and on the type of ion-ion interaction (through h). If the thickness of the structure increases, the lower value of μ increases too.

For simplification, instead of the expression (20), we will use the approximate expressions for energies, which we obtain by the expansion of the square root up to the quadratic terms:

$$E_1 = E_z^{(0)} + 4b^2(2\mu+1)^2\Phi W_z - \frac{W_z}{2(2\mu+1)^2 b^2 \Phi} \qquad (23)$$

and

$$E_2 = E_z^{(0)} + \frac{W_z}{2(2\mu+1)^2 b^2 \Phi}. \qquad (24)$$

It is very easy to notice that both obtained expressions for energies satisfy the necessary condition (18). However, by the analysis of (22) and (23), we can conclude the following.

- Since $E_2 < E_1$, the states with energy E_2 are more stable and more populated and so they essentialy define the normal behavior of the system.
- From the expressions (21) and (23) it follows that the increase of film thickness (the increase of N_z) causes the increase of the lower boundary of the index μ, and the correction of E_2, which depends on sputtering, decreases. This is in complete agreement with the conclusions that we can accomplish without going over to continuum, i.e. directly analysing discrete eq.s (15).

We can see in expressions defining ζ – text under (18), that the boundaries of the interval for ζ are proportional to $L/\bar{a}_z = b^{-1}$ and so we can approximately take: $\zeta \in [-\infty, +\infty]$, where the approximation is better if the film is thicker. We can then express the solutions of equation (19) using Hermite polynomials:

$$A_\mu(\zeta) = \frac{e^{-\zeta^2/2}}{\left(2^\mu \mu!\sqrt{\pi}\right)^{1/2}} H_\mu(\zeta)\;; \quad H_\mu(\zeta) = (-1)^\mu e^{\zeta^2}\frac{d^\mu}{d\zeta^\mu}(e^{-\zeta^2}) \quad \mu = 0,1,2,\ldots \qquad (25)$$

In this way we have defined single-particle degenerate states of the system: for the wave functions – by the equations (12), (14), and (24) and for energies – by (20).

4. CHARGE CARRIERS DISPERSION LAW

We shall perform the diagonalization of the electron Hamiltonian in the following stages.

1. In the framework of the continual approximation, Hamiltonian H_B "melted" in Hamiltonian H_V using the formulas for transition to continuum

$$C_{n_xn_yn_z} \to C_{n_xn_y}(\zeta); \qquad W_z\left[1+\frac{4\Phi}{L^2}\left(z-\frac{L}{2}\right)^2\right] \to W_z\left(1+\frac{4\Phi\tau_\mu}{L^2}\zeta^2\right).$$

(Because of the transformation $n_z \to z \to \tau\zeta$, it is obvious that the sum over n_z must be changed by integral over ζ: $\sum_{n_xn_yn_z} \longrightarrow \tau\bar{a}_z^{-1}\sum_{n_xn_y}\int_{-\infty}^{\infty}d\zeta$).

2. From the operators $C_{n_xn_y}(\zeta)$ we go over to new operators $C_{k_xk_y\mu}$ using the canonical transformations:

$$C_{n_xn_y}(\zeta) = \sum_{k_xk_y\mu} A_{n_xn_y}^{k_xk_y}(\mu,\zeta)C_{k_xk_y\mu}. \tag{26}$$

Therefore we can write Hamiltonian H_V in the continual approximation in the form:

$$\begin{aligned} H_V \longrightarrow H = \frac{\tau}{a_z}\sum_{n_xn_y}\int_{-\infty}^{\infty}d\zeta C_{n_xn_y}^{+}(\zeta)\Big\{\Lambda C_{n_xn_y}(\zeta) - \\ -W_x\left[C_{n_x+1,n_y}(\zeta)+C_{n_x-1,n_y}(\zeta)\right] - W_y\left[C_{n_xn_y+1}(\zeta)+C_{n_xn_y-1}(\zeta)\right] - \\ -W_z\left(1+\frac{4\Phi\tau^2}{L^2}\zeta^2\right)\left[2C_{n_xn_y}(\zeta)+\frac{\bar{a}_z^2}{\tau^2}\frac{d^2C_{n_xn_y}(\zeta)}{d\zeta^2}\right]\Big\}. \end{aligned} \tag{27}$$

We can now perform the diagonalization of Hamiltonian. After the substitutions (26) into (27) we have:

$$\begin{aligned} H = \frac{\tau}{\bar{a}_z}\sum_{k_xk_y\mu}\sum_{q_xq_y\nu}C_{q_xq_y\nu}^{+}C_{k_xk_y\mu}\sum_{n_xn_y}\int_{-\infty}^{\infty}d\zeta\left[A_{n_xn_y}^{q_xq_y}(\nu;\zeta)\right]^*\Big\{\Lambda A_{n_xn_y}^{k_xk_y}(\mu;\zeta) - \\ -2W_x\left[A_{n_x+1,n_y}^{k_xk_y}(\mu;\zeta)+A_{n_x-1,n_y}^{k_xk_y}(\mu;\zeta)\right] - 2W_y\left[A_{n_xn_y+1}^{k_xk_y}(\mu;\zeta)+A_{n_xn_y-1}^{k_xk_y}(\mu;\zeta)\right] - \\ -2W_z\left(1+\frac{4\Phi^{\ 2}}{L^2}\zeta^2\right)\left[2A_{n_xn_y}^{k_xk_y}(\mu;\zeta)+\frac{\bar{a}_z^2}{\tau^2}\frac{d^2A_{n_xn_y}^{k_xk_y}(\mu;\zeta)}{d\zeta^2}\right]\Big\}. \end{aligned} \tag{28}$$

Based on (14) one can write: $A_{n_j+1}^{k_xk_y}(\mu;\zeta)+A_{n_j-1}^{k_xk_y}(\mu;\zeta) = 2\,A_{n_xn_y}^{k_xk_y}(\mu;\zeta)\cos(a_jk_j), \quad j=(x,y)$. If we substitute E with $E_{k_xk_y\mu}$ and z with ζ in the last of (15), we find $W_z(1+\frac{4\Phi\tau^2}{L^2}\zeta^2)\left[2A_\mu(\zeta)+\frac{\bar{a}_z^2}{\tau^2}\frac{d^2A_\mu(\zeta)}{d\zeta^2}\right] = \left(E_z^{(0)}-E_{k_xk_y\mu}\right)A_\mu(\zeta)$, which yields

$$W_z\left(1+\frac{4\Phi\tau^2}{L^2}\zeta^2\right)\left[2A_{n_xn_y}^{k_xk_y}(\mu;\zeta)+\frac{\bar{a}_z^2}{\tau^2}\frac{d^2A_{n_xn_y}^{k_xk_y}(\mu;\zeta)}{d\zeta^2}\right] = \left(E_z^{(0)}-E_{k_xk_y\mu}\right)A_{n_xn_y}^{k_xk_y}(\mu;\zeta).$$

Using this and the orthonormalization condition from (12), we diagonalize the expression (28) for the Hamiltonian of the system:

$$H = \sum_{k_xk_y\mu}E_{k_xk_y\mu}C_{k_xk_y\mu}^{+}C_{k_xk_y\mu}. \tag{29}$$

This expression represents the Hamiltonian of the electron subsystem which was the subject of this study. Together with the Hamiltonian of the phonon subsystem derived earlier [5–7], it enables the continuation of the investigation of the superconductivity mechanism in high-temperature oxide ceramics. Analyses performed until now enable us to conclude that the theoretical model of symmetrically deformed structures satisfies the basic experimental indicators of superconductive perovskite behavior. It is primarily related to the proven presence of a gap in the spectrum of elementary excitations in this system (phonons or electrons) and its behavior in the structures with different stoichiometry. The question of the interaction between the subsystem of elementary charges and the subsystem of phonons (optical type) is still open; this question is crucial for the understanding of the nature of the new superconductive state.

5. ESTIMATE OF SYSTEM ORDERING

In this section of the paper, we shall analyse the Landau superfluidity criterion and determine the probabilities of states and entropy of the system. Landau criterion for superfluid motion is $\min v > 0$, where $v = E(p)/p$. The expression for energies (20) (using the approximations: $a_x \cong a_y \equiv a$, $a_z \cong 3a$, $W_x \cong W_y \equiv W$, $W_z = W/3^h$, $\sin\alpha \simeq \alpha$, $k_x = k\sin\theta\cos\varphi$, $k_y = k\sin\theta\sin\varphi$, $k_z = k\cos\theta$) yields the following expression:

$$E_{1;2}(p) = \frac{Wa^2}{\hbar^2}\left[p^2\sin^2\theta + g_{\pm}^2(\mu)\right], \qquad (30)$$

where $g_{\pm}^2(\mu) = 2\,3^{-h}\hbar^2 a^{-2} f^2(\mu)\left[1 \pm \sqrt{1-2f^{-2}(\mu)}\right]$; $f^2(\mu) = b^2(2\mu+1)^2\Phi$. For the phase velocity, we get:

$$v_{1;2}(p) = \frac{E_{1;2}(p)}{p} = \frac{Wa^2}{\hbar^2}\left[p\,\sin^2\theta + \frac{1}{p}g_{\pm}^2(\mu)\right] \qquad .(31)$$

The condition $dv/dp = 0$ yields $p_e = g_{\pm}(\mu)\sin^{-1}\theta$. Because of $\theta \in [0,\pi] \Rightarrow v_{1,2}^2 \geq 0$, and because $g_+ \geq g_- \Rightarrow v_1^2 \geq v_2^2$. It follows that the state with the energy E_1 has a more expressive minimum than the state with the energy E_2. For the second derivative, we get:

$$\frac{d^2v_{1;2}}{dp^2}|_{p=p_e} = 2Wa^2\hbar^{-2}\,g_{\pm}^{-1}(\mu)\sin^3\theta \;\geq\; 0. \qquad (32)$$

We can see that the known − Landau criterion is satisfied for both energies, but it is "stronger" for the states with the energies E_1 ($\geq E_2$) because E_1 has a bigger gap than E_2.

We shall now determine the probability of the state of the system under consideration. If we introduce the notation

$$\epsilon_{1;2} \equiv E_{1;2} - E_z^{(0)} = 2W_z\left[3^h a^2\hbar^{-2}g_{pm}^2(\mu) - 1\right], \qquad (33)$$

we can find − see text under the (18):

$$\tau_{1;2} = \left(\frac{\bar{a}_z}{2}L\right)^{1/2}\left(\Phi\epsilon_{1;2}W_z^{-1}\right)^{-1/4} \qquad .(34)$$

Then the wave function (12) has the form:

$$\Psi_{1;2}(k_x,k_y,k_z) = \frac{\tau_{1;2}}{\bar{a}_z}\sum_{n_xn_y}\int_{-\infty}^{+\infty} d\zeta |A_{n_xn_y}^{k_xk_y}(\mu;\zeta)|_{1;2}\, C_{n_xn_y}^{+}\,|0\rangle \qquad (35)$$

where $|A_{n_xn_y}^{k_xk_y}(\mu;\zeta)|_{1;2} = N_{1;2}\,e^{i(n_xa_xk_x+n_ya_yk_y)}A_\mu(\zeta)$ and norm-factor is defined on the following way $N_{1;2} = \bar{a}_z\left(N_xN_y\tau_{1;2}\right)^{-1}$. The probability of finding the elementary charges with the energy E_1 (and E_2), in agreement with (35), is:

$$P_{1;2}(\mu;\zeta) = \left(\frac{\tau_{1;2}}{\bar{a}_z}\right)^2 |A_{n_xn_y}^{k_xk_y}(\mu;\zeta)|_{1;2}^2 = N_x^{-2}N_y^{-2}\,A_\mu^2(\zeta), \qquad (36)$$

wherefrom:

$$P_1(\mu;\zeta) = P_2(\mu;\zeta) \equiv P_\mu(\zeta). \qquad (37)$$

Based on the last expression we can see that both states appear with equal probabilities!

The entropy of the system under consideration is:

$$S_{1;2}(\mu) = -\frac{\tau_{1;2}}{\bar{a}_z}I(\mu), \qquad (38)$$

where the integral $I(\mu) \equiv \int_{-\infty}^{+\infty} d\zeta P_\mu(\zeta)\ln P_\mu(\zeta)$ is need not be calculated, since, from (4.9) and (34), it follows:

$$\frac{S_1(\mu)}{S_2(\mu)} = \frac{\tau_1}{\tau_2} \equiv \left(\frac{\epsilon_2}{\epsilon_1}\right)^{1/4} \leq 1 \;\Rightarrow\; S_1(\mu) \leq S_2(\mu). \qquad (39)$$

(Since $E_1 \geq E_2$, we get $\epsilon_{1;2} \geq 0$ and $\epsilon_1 \geq \epsilon_2$). This expression yields that the states Ψ_2 (with E_2) are less ordered than the states Ψ_1 (with E_1). It means that the states with E_1 (with higher energy and lower population) are probably responsible for superconductive effects in the observed system. The states with E_2 (with lower energy and higher population) are responsible for the normal behavior of this system. This is in agreement with the above comments about these two possible energies

6. CONCLUSION REMARKS

The particular features of high-temperature superconductors based on oxide ceramics are their granular structure and the anisotropy of properties. The existence of the weak isotopic effect and Cooper pairs of charge carriers is experimentally verified, similar to the conventional superconductors, but the BCS model could not explain high critical

temperature. For that reason and based on established experimental results [1–3,13–15], we have proposed the model of ceramic structure as tetragonal i.e. generalised cubic structure in which interatomic distances along one direction are a few times bigger than along the other two directions. It is, energetically, most convenient if the sputtered atoms locate themselves just along this direction.

The analysis of the phonon spectrum in our model yields that we have phonon branches of optical type only in the spectrum (there exists an energy gap). It means that for phonon excitation the energy (heat) must be bigger than the energy gap.

The analysis of the electron spectrum in these symmetrically deformed structures (concerning the planes $n_z = 0$ and $n_z = N_z$) yields that, as a consequence of the existence of the boundaries along z axes, we have two energy branches in the spectrum of charge carriers. The lower energy value is related to more populated states and contains the term depending on the sputtering. This term decreases with increasing of the film thickness. The higher energy value in the spectrum of charge carriers is not particularly analysed because these levels are low populated.

In addition to this, in the framework of the model under consideration, we have determined the orthonormalized single-particle state functions of this system, entropy, and the probabilities of possible states. The theoretical investigation in the framework of the presented model is not finished. It is necessary to form a Hamiltonian of the interaction between charge carriers and phonons and separate from it the essential part only, which describes the formation of Cooper pairs. Only after this, the thermodynamical analysis of the complete system follows.

Acknowledgments

The research presented in this paper was financially supported by the Ministry of Scientific and Technological Development, Higher Education and Information Society of the Republic of Srpska (Projects No. 19.032/961-36/19 and 19.032/961-42/19).

Conflicts of Interest

The authors declare no conflict of interest.

7. REFERENCES

[1] J. G. Bednorz and K. A. Müller, *Perovskite-Type Oxides* – the New Approach to High-T_c Superconductivity; *Nobel Lecture,* Stockholm, December 8, 1987

[2] P. H. Hor et.al, Superconductivity above 90 K in the square-planar compound system ABa$_2$Cu$_3$O$_{6+x}$ with A=Y,La,Nd,Sm,Eu,Gd,Ho,Er and Lu, *Phys.Rev.Lett.* , 58 (1987) 1891

[3] A. A. Abrikosov, Theory of High–Tc Superconducting Cuprates Based on Experimental Evidence, http://www.lanl.gov./find/cond.mat, (1999) 9912394

[4] N. M. Plakida, High - Temperature Superconductors, *Springer - Verlag*, Berlin 1995

[5] B. S. Tošić, J. P. Šetrajčić, R. P. Djajić and D. Lj. Mirjanić, Phonons in Broken-Symmetry Structures, *Phys.Rev.* B, 36, (1987) 9094

[6] J. P. Šetrajčić, R. P. Djajić, D. Lj. Mirjanić and B. S. Tošić, Phonon Spectra in Superconducting Ceramics, *Phys.Scr.*, 42 (1990) 732

[7] J. P. Šetrajčić, V. M. Zorić, N. V. Delić, D. Lj. Mirjanić and S. K. Jaćimovski, Phonon Participation in Thermodynamics and Superconductive Properties of Thin Ceramic Films, Chapter 15, pp. 317-348, In „Thermodynamics", Ed.M.Tadashi, ISBN: 978-953-307-544-0, *InTech*, Vienna (Austria) 2011; Available from: http://www.intechopen.com/articles/show/title/phonon-participation-in-thermodynamics-and-superconductive-properties-of-thin-ceramic-films.

[8] J. P. Šetrajčić, S. M. Vučenović and S. K. Jaćimovski, Possible States of Charge Carriers in Thin Multilayered Superconductive Ceramics, *Zaštita Materijala* 57(2016)2, pp. 239-243

[9] S. M. Vučenović, J. P. Šetrajčić and D. I. Ilić, Superconductivity of Lanthanum Hydride to 250 K, *Proceedings 12th ContMat* (ISBN 978-99976-42-30-1), 2020, pp. 91-103

[10] Ch. Kittel, *Introduction to Solid State Physics*, *Wiley*, New York 2004

[11] P. Hoffmann, *Solid State Physics*, Wiley, New York 2015.

[12] S. M. Girvin and K. Yang, *Modern Condensed Matter Physics*, Univ.Press, Cambridge Cambridge, 2019

[13] R. Simon, High-*T*c Thin Film and Electronic Devices, *Physics Today,* 44 (1991) 64

[14] D. R. Harshman and A. P. Mills, *Phys.Rev. B* 45 (1992), 10684

[15] W. E. Pickett, *Rev.Mod.Phys.,* 61(1989), 433

JST&M 6(2024), 8 - 14
DOI: 10.57131/jstm.2024.6.2

Original scientific paper

THE EFECT OF DIMENSIONALITY AND CURRENT STRENGHT ON CONDUCTIVITY OF GRANULAR METALS

[1]Maja Đekić, [1]Ajla Karić, [1]Amra Salčinović Fetić, [1]Melisa Baždar, [1]Belma Husković, [2]Dijana Dujak
[3]Diana Ćubela

[1]University of Sarajevo, Faculty of Science, [2]University of Sarajevo, Faculty of Electrical Engineering, University of Zenica, Faculty of Engineering and Natural Science

ABSTRACT

Metallic materials in granular packings show different electrical properties from their bulk counterparts. In this paper, we investigate the temporal evolution of the electrical conductivity of granular metals. We use metallic beads arranged in different one-, two- and three-dimensional ensembles through which different constant currents are injected. The conductivity behavior in all three types of systems is qualitatively similar. The results show the rise of conductivity which is more pronounced in the earlier stages of the time evolution. We investigate the influence of the dimensionality, number of the beads, and the values of the injected currents on the conductivity behavior.

Keywords: granular metals, electrical resistance, weak contacts

Corresponding Author:
Maja Đekić,
University of Sarajevo, Faculty of Science
Zmaja od Bosne, University Campus, 71 000 Sarajevo, B&H
Tel.: +387 033 279 891387.
E-mail address: mdjekic@pmf.unsa.ba

1. INTRODUCTION

Granular metals display quite unique electrical resistance behavior when compared to their bulk counterparts. For any conducting wire, the resistance is proportional to its length and inversely proportional to its cross-section area while it remains constant in time. In granular metals, the resistance is caused by both the individual resistance of the grains as well as by the contacts between them [1]. A few authors have recorded the decrease in resistance with time in granular metals [2, 3, 4] which is more pronounced in the earlier stages of the time evolution. The origin of this phenomenon can be found in the theory of contact resistance. Because every surface has some roughness either on micro or even nano scales, the electrical contact between the granules is established through discrete spots, known as a-spots or asperities which determine the actual size of the contact area. It is usually much smaller than the nominal contact area [5]. This affects the electromechanical properties of the materials due to the large pressure exerted on these spots. Contact resistance can also originate from the tunneling, especially in metallic powders covered with thin oxide layers [2]. Over the years, many theoretical models have been developed to model contact resistance. However, most of them include major simplifications ignoring correlations between asperities, roughness of the surface, or existence of the oxide layer [6, 7]

Various authors suggest that the number of beads, temperature, vibrations, packing, and applied force [8, 9] can also influence the

electrical properties of these materials. According to [10], the properties of the granular materials seem to be universal i.e. independent of the type and size of the grains, but are rather attributed to the granular structure of the system itself.

In this paper, we measure a flow of different fixed currents through 1D, 2D, and 3D compact packings of steel cylinders to examine the effect of dimensionality, the number of cylinders, and the current value on the resistance behavior.

2. EXPERIMENTAL PROCEDURE

The schematic of the experimental setup is shown in Figure 1.

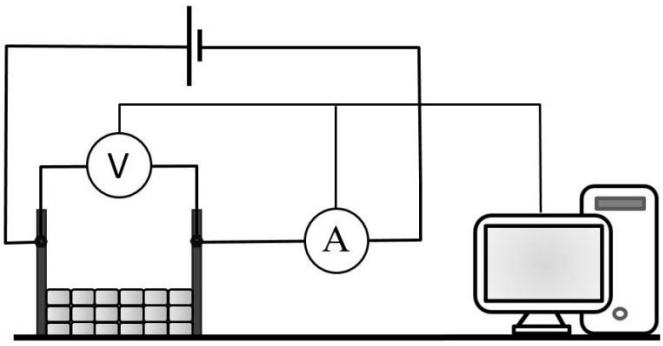

Figure 1. Sketch of the experimental setup. The current is injected into the cylinder packing. The voltage and the current are registered and the resistance is calculated

The steel cylinders with a diameter of 5 mm are placed in an isolating box with plate electrodes on the side walls. The box is placed under a small inclination angle of 15° onto an anti-vibration table. A fixed current is injected into a cylinder packing from a current source Kiethley 228, while the current and voltage are measured with Multimetars GDM 8621A (GW – Instek). The data is acquired by a computer program that calculates resistance using Ohm's law. The temperature is measured using PeakTech digital thermometer. Small variations between 1-2 °C are recorded and do not seem to alter the behavior of resistance.

The cylinders were first arranged in a 1D linear chain containing 18 beads (Figure 2 a) and a fixed current between 10 mA and 80 mA was imposed onto the chain for 600 s with 10 s step. For every fixed current value, a set of five measurements has been conducted in the following manner: After each measurement, new contacts between the cylinders were established by reducing the current to zero, removing the cylinders from the box, and after a couple of minutes placing them back to the same place as before, thus creating a new packing of cylinders for every measurement.

2D packings of cylinders were formed by placing them in rows, starting from two rows up to ten rows (Figure 2 b), thus containing 36 to 180 beads respectively. The current injected into 2D packings was 50 mA and one measurement was conducted for each number of rows. The current and voltage were measured and recorded every 10 s for 300 s.

3D packings were formed by placing the cylinders into rows and columns 3 by 3 (162 beads), 5 by 3 (270 beads), and 7 by 3 (378 beads) with 50 mA current injected into them (Figure 2 c). The current and voltage were measured every 10 s for 300 s. Note that for 2D and 3D arrangements of cylinders, new contacts were established after each measurement.

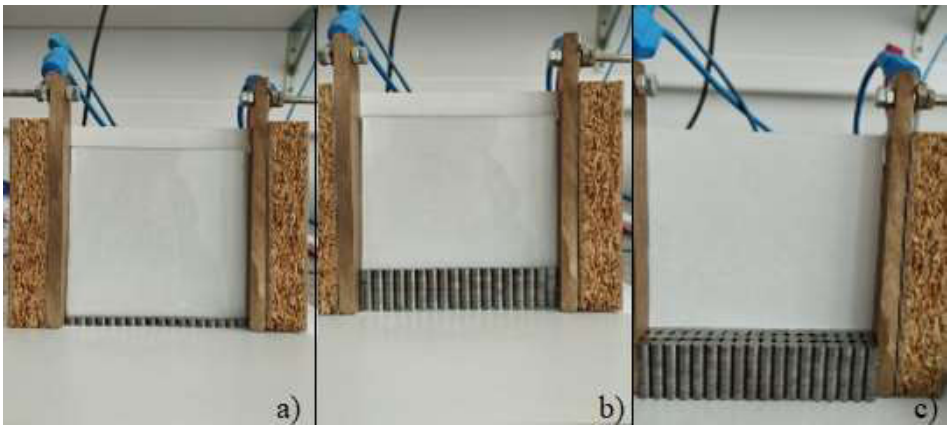

Figure 2. a) 1D packing b) 2D packing containing 6 rows and c) 3D packing containing five rows and three columns of the cylinders

Scanning electron microscopy (SEM) was performed using JEOL JSM IT 200LA while atomic force microscopy (AFM) imaging was performed using Nanosurf CoreAFM. AFM imaging was acquired in dynamic mode using Nanosurf DynAl-900 tips (nom. freq. 190 kHz, nom. force const. 48 N/m) with linear scanning time of 1 s and scan resolution of 256 points per line. The measurements were performed in air ambient temperature and humidity. Analysis of the images was carried out using WsXM software [11].

3. RESULTS AND DISCUSSION

Typical behavior of the electrical conductivity σ in a 1D linear chain is presented in Figure 3.

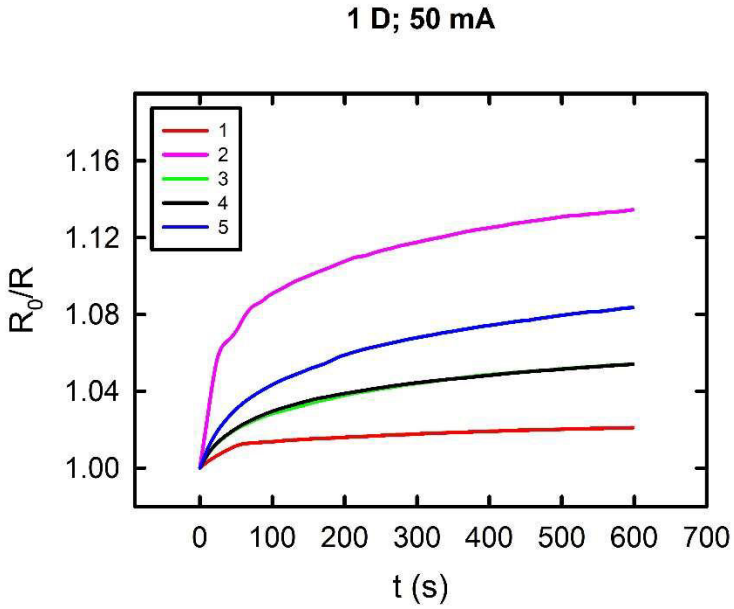

Figure 3. Five measurements of the normalized conductivity ($\sigma=R_0/R$, where R_0 is the initial resistance and R is the measured resistance) for 50 mA current injected into the 1D chain

Five measurements of conductivity were performed for 50 mA current injected into the 1D chain of cylinders. Before each new measurement, a new packing of cylinders was created following the procedure as previously explained in the experimental section of this article. According to our results (Figure 3), electrical conductivity rises with

time which is more pronounced in the earlier stages of the experiment. Also, the initial value of the resistance as well as the rate of the resistance change for every packing, which had been previously established and can be attributed to the establishment of new microcontacts between the cylinders [4].

Qualitatively, the electrical conductivity in 2D arrangements of cylinders (Figure 4) is similar to the one in 1D linear chains.

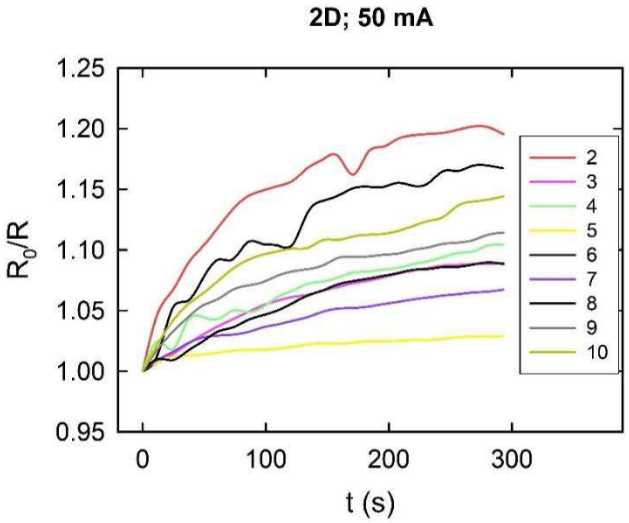

Figure 4. Normalized conductivity ($\sigma=R_0/R$, where R_0 is the initial resistance and R is the measured resistance) for 50 mA current injected into the 2D packings containing from 2 to 10 rows

This unusual result can be understood when analyzing the current paths in 2D systems. According to [12] the current in 2D systems seems to be localized in desecrate linear paths regardless of the strength of the injected current.

3D packings display similar conductivity behavior as 1D and 2D systems, as illustrated in Figure 5.

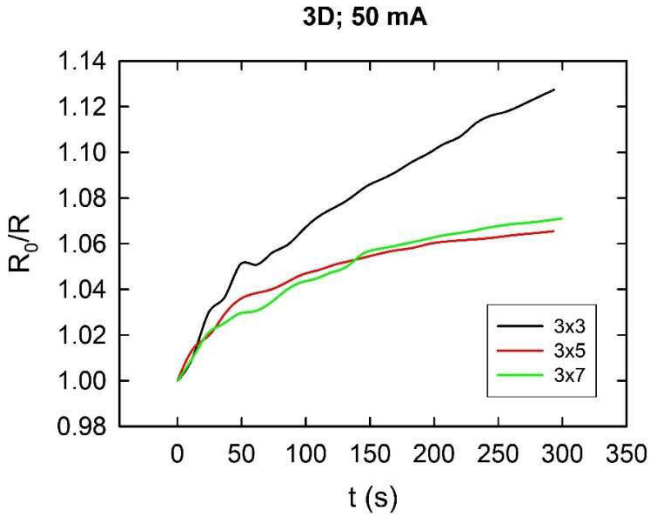

Figure 5. Normalized conductivity ($\sigma=R_0/R$, where R_0 is the initial resistance and R is the measured resistance) for 50 mA current injected into the 3D packings of cylinders

According to our results, dimensionality does not seem to influence the behavior of the time evolution of conductivity in granular metals because the current seems to stay localized in linear paths.

Next, we examine the current strength on the conductivity behavior. Since all the packings

regardless of the dimensionality display similar behavior, we examined only 1D packings of cylinders for the current values between 10 mA and 80 mA, as presented in Figure 6.

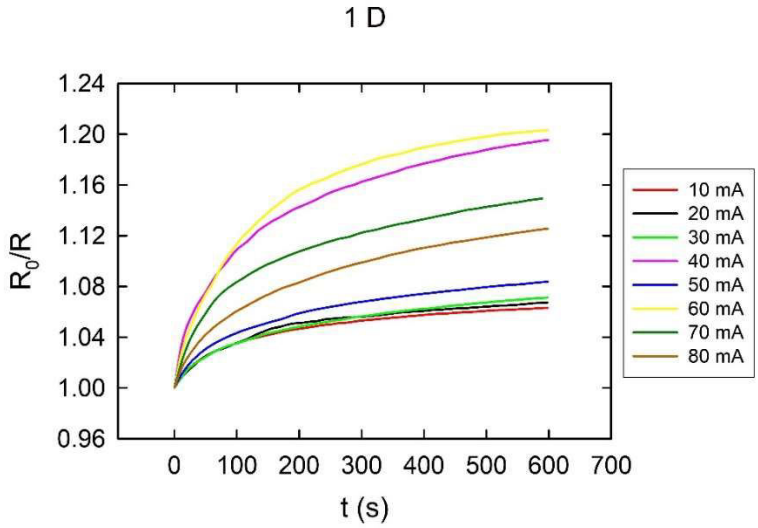

Figure 6. Normalized conductivity ($\sigma=R_0/R$, where R_0 is the initial resistance and R is the measured resistance) for currents between 10 mA and 80 mA injected into the linear chain of cylinders

Qualitatively, the conductivity behaves in the same manner for all the current values. The initial values of conductivity and the rates of conductivity rise do not seem to correlate with the current strength. Namely, for each stronger current imposed on the system, the initial conductivity can either be smaller or larger than for the previously imposed weaker current. According to our measurements, the most significant influence on conductivity seems to be originating from the contact resistance which is greatly affected by the cylinders' surfaces. To examine the cylinder surfaces, SEM imaging, presented in Figure 7 was performed. The surface showed visible scratches due to the cutting.

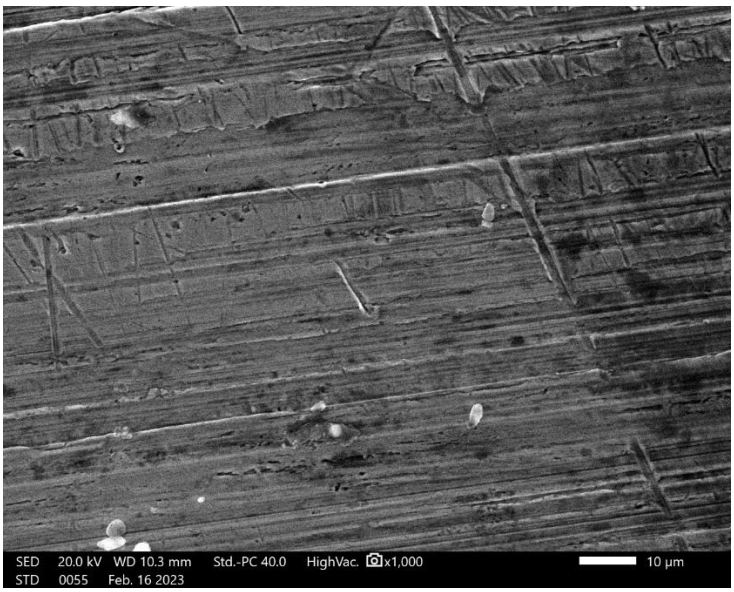

Figure 7. SEM image of the cyllinder surface

To examine the topography of the cylinders, AFM imaging was conducted. Figure 8 represents a 3D image of a flat surface of one cylinder. The image revealed needle-like asperities and also some deep furrows. Surface roughness is 93 nm rms, but the differences in height are rather pronounced and go up to 592 nm in some places.

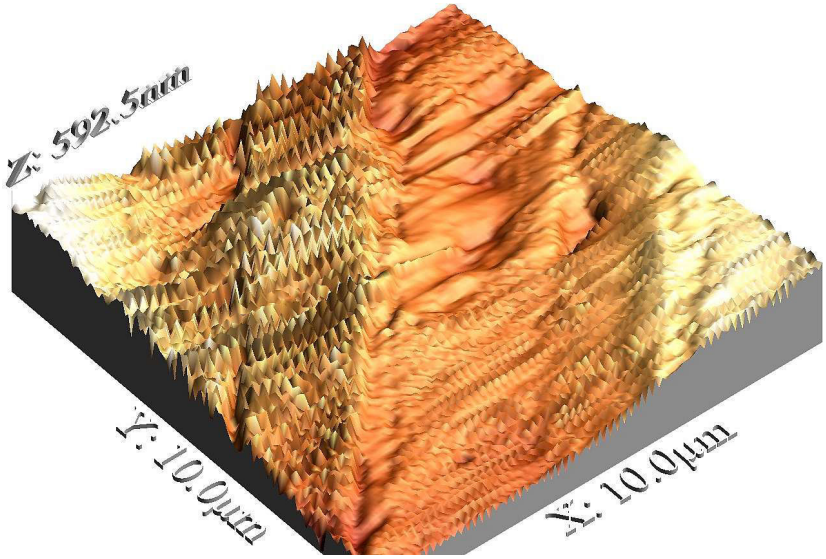

Figure 8. 3D image of the cyllinder surface

4. CONCLUSION

Our results show that in granular ensembles of steel metallic cylinders, the conductivity rises with time regardless of the dimensionality or the current strength injected into them. A similar trend was observed in other granular systems of different metals. This may be attributed to the granular nature of the material itself, which seems to not depend on the dimensionality, number of grains, shape, size, or even grain material. A predominant factor in this behavior originates from the contact resistance which is associated with the number and height of asperities as well as with the oxide layers on the metallic surface. AFM measurements of our samples revealed very rough samples with a lot of needle-shaped asperities. The highest of them contribute to conductivity, while the shorter ones, especially if they are in the furrows, probably do not influence the conductivity. To investigate whether it is possible to influence the conductivity behavior with mechanical treatment of the surface of the cylinders, in our next experiments we are planning to measure conductivity after polishing.

Conflicts of Interest

The authors declare no conflict of interest.

5. REFERENCES

[1] R. Holm, Electric contacts: Theory and Application, Springer-Verlag Berlin Heidelberg New York, 1967

[2] Z. M. Jakšić et al., The Electrical Conductance Growth of a Metallic Granular Packing, *Eur. Phys. J. B,* 90 (2017) 108,

[3] S. Dorbolo et al., Aging Process of Electrical Contacts in Granular Matter, *Journal of Applied Physics*, 94 (2003) 12

[4] D. Dujak et al., Temporal Evolution of Electrical Resistance through Granular Packing of Ni Beads, *Bulliten of Chemists and Technologists of Bosnia and Herzegovina*, 58(2022), pp. 33-38

[5] L. Hirpa, Gergele et al., Study of Contact Area and Resistance in Contact Desing of Tubing Connections, 13th International Research/Expert Conference "Trends in the Development of Machinery and Associated Technology", TMT, Hammamet, Tunisia, 2009

[6] K. Bourbatache et al., Discrete Modeling of Electrical Transfer in Multi-Contact Systems, *Granular Matter*, 14 (2012), pp. 1-10

[7] B. F. Toler et al., A Review of Micro-Contact Physics for Microelectromechanical Systems

(MEMS) Metal Contact Switches, *J. Micromech. Microeng.,* 23, 2013

[8] S. S. Yoon et al., Pattern Formations in Granular Systems and Their Implications to Dynamics of Ferroelectrics, *J. Korean Phys. Soc.,* 35 (1999) S1326,

[9] E. Falcon et al., Nonlinear Electrical Conductivity in a 1D Granular Medium, *Eur. Phys. J. B* ,38 (2004),pp. 475-483

[10] M. Massalska-Arodź et al., Experimental Observations of Structural Relaxation in Granular Matter, *Physical Review E*, 55 (1997) 1

[11] I. Horcas et al., WSXM: A software for scanning probe microscopy and a tool for nanotechnology, *Review of Scientific Instruments*, 78 (2007), 013705

[12] M. Creyssels et al., Some Aspects of Electrical Conduction in Granular Systems of Various Dimensions, *Eur. Phys. J. E* 23(2007), pp. 255-264

JST&M 6(2024), 15-21
DOI: 10.57131/jstm.2024.6.3

Original scientific paper

EFFECT OF CHROMIUM CONTENT ON MECHANICAL PROPERTIES OF NICKEL-FREE AUSTENITIC STAINLESS STEELS

Jasmin Halilović[1], Edis Nasić[1], and Derviš Mujagić[2]

[1]University of Tuzla, Faculty of Mechanical Engineering, [2]University of Zenica, Institute "Kemal Kapetanović"

ABSTRACT

This study investigated the mechanical properties of a series of Fe-Cr-Mn (Mo)-N alloys. The chromium content ranged from 16 to 18 mass%. The test alloys were produced by adding nitrided ferroalloys during melting in an induction furnace. Test specimens of each alloy were prepared for mechanical testing and microstructural observation. Tensile strength (TS) and elongation (EL) were determined. By increasing or decreasing the content of the chromium, it can directly affected on the values of the mechanical properties and the final microstructure. A series of experiments showed that increasing the chromium content by 1.46 mass% in the Fe-16Cr-8Mn (Mo)-N alloy led to a decrease in the TS value by 12% and in the EL value by 16.1%, while increasing the chromium content by 0.72 mass% in the Fe-16Cr-11Mn (Mo)-N alloy caused a decrease in the TS value by 6.1% and in the EL value by 16%. The chromium content of 16 mass % in the studied alloys was found to provide sufficient strength and a relatively high elongation value. The alloys can also contain a higher mass fraction of chromium, but to obtain a complete austenitic structure it is necessary to increase the content of manganese and nitrogen.

Keywords: chromium; nitrogen; mechanical properties; tensile strength; elongation

Corresponding Author:
Jasmin Halilović,
University of Tuzla, Faculty of Mechanical Engineering
Urfeta Vejzagića 4, 75000 Tuzla, B&H
Tel. +387 61 660 227; fax: +387 32 320 921.
E-mail address: jasmin.halilovic@untz.ba; jasmin.halilovic.msf@gmail.com

1. INTRODUCTION

Stainless properties are provided by chromium which, together with oxygen from the air, creates a thin, hard, and compact layer of chromium oxide Cr_2O_3 on the surface which protects the metal from further corrosion. In case this surface layer gets damaged, it is recreated in the damaged area. For the protective layer to be formed, the chromium content in the steel must be at least 12.5% according to previous statements, however, this limit has been reduced to 10.5% per BAS EN 10020:2000 [1].

Another condition of anti-corrosion is the monophase microstructure. This condition does not necessarily have to be met. Most stainless steels have monophase microstructure, but there are some whose microstructure is composed of two or more phases.

The ratio of alphagenic and gammagenic alloying elements affects the formation of the final microstructure. It is known that chromium, silicon and molybdenum promote ferritic microstructure. In most cases the total mass fraction of gammagenic alloying elements in austenitic stainless steels is greater than 8% [2]. Nickel in the alloy is completely substituted with manganese and nitrogen. Nitrogen is added as an alloying element. Manganese significantly increases solubility of nitrogen [2,3]. Furthermore, to improve the corrosion resistance of this alloy, molybdenum was added (2-3%) [2,3].

Besides the effect of chemical composition on the formation of microstructure, a significant role is played by subsequent solution annealing heat treatment. It is known that usage of stainless austenitic steels at elevated temperatures is accompanied by the precipitation of phases, many of which worsen the mechanical and anti-corrosive properties. If chromium and molybdenum in the alloy are present in large quantities, there is a danger that brittle, intermetallic phases can be formed [1].

The three most common intermetallic phases found in austenitic stainless steels are the sigma phase, chi phase, and Laves phase [4]. For steels with nitrogen content over 0.2%, chromium nitrides can precipitate at the grain boundaries, as well as inside the grain [5]. In most cases, after the casting and cooling, chromium nitrides are formed in the austenitic microstructure matrix wherefore it is necessary to perform solution annealing heat treatment to eliminate nitrides and also intermetallic phases. Besides the precipitates mentioned above, it is important to note that, depending on chemical composition and parameters of heat treatment, sometimes delta (δ) ferrite can be found in the austenitic matrix. Delta ferrite is also commonly found in cast ingots that have not been subjected to subsequent heat treatment. According to all the above, it can be concluded that the production process of nickel-free austenitic steels is highly complex, and that the mechanical properties of such steels are highly influenced by the chemical composition of the alloy, production and heat treatment parameters.

Since the alloy is completely nickel-free, it is considered as pleasant for the human body (does not cause allergic reactions) and it is commonly used for jewelry, wristwatches, dental covers, coronary stents and more [6,7]. In the latest world references, there are several papers concerning the role of chemical composition, crystallization conditions and heat treatment in the formation of nickel-free austenitic steel microstructure. The formation of microstructure is highly influenced by changing the fraction of any chemical element in the Fe-Cr-Mn (Mo)-N austenitic steels, which affects the mechanical properties of those steels as well. In this paper, the results of research of the influence of chromium on the microstructure and mechanical properties of nickel-free austenitic steel are presented.

2. EXPERIMENTAL RESEARCH, RESULTS AND DISCUSSION

Nitriding of alloys are seen as complex technical and technological tasks. Nitriding of alloys can be split into two groups.

The first group is composed of processes in which melted alloy is saturated with nitrogen in the form of gas. In the second group of processes, the nitrogen content is increased by adding solid metals or ferroalloys, which contain nitrogen and are added to the melted alloy. Then, nitrogen passes into the melt [1,8,9].

Nitrated alloys present in this paper have been produced using an induction furnace, while the introduction of nitrogen into the steel was done by adding nitrated ferroalloys (Cr, Mo, Mn, high nitrogen ferro-chrome) in various ratios, in order to obtain the desired chemical composition of the ingots. ARMCO iron produced in an open induction furnace was used as a basic charge. Considering that the alloying of melt was carried out under atmospheric pressure, the solubility of nitrogen is limited to 0.5%N. Also, using this production process, it is difficult to obtain alloys with a homogeneous chemical composition, whereforethe obtained ingots are subjected to hot forging to reduce the thickness by 50-80%. After forging, water jet cutting was performed to obtain pieces with dimensions of 95x35x25 mm(three pieces for each alloy), which were subjected to solution annealing at 1100°C for 60 min, and water quenched. The chemical composition of the obtained ingots - austenitic stainless steels is given in Table 1, and it was determined on a spectrometer of the PolySpek series. In addition to the chemical analysis on the spectrometer, a microchemical analysis was also performed on some samples, to determine the phases and their chemical composition. Metallographic analysis of the samples was performed using a light microscope (Olympus GX53) according to the

BAS EN ISO 17639:2023 standard. Then the content of delta ferrite and precipitates was assessed using the modified software OptikaISView and ImageJ - for phase analysis of the microstructure. Testing of mechanical properties was performed on test pieces prepared by EN 10002-1 - tensile testing at room temperature.

Table 1. Composition of austenitic stainless steels (mass%)

Alloy	Cr	Mn	Mo	Si	Ni	N
A1	16.2	8.33	2.94	0.106	≤0.1	0.38
A2	17.66	8.40	2.91	0.105	≤0.1	0.42
A3	15.96	10.85	3.49	0.083	≤0.1	0.27
A4	16.68	10.54	3.45	0.101	≤0.1	0.23

2.1. Mechanical properties

After the completion of the forging process and subsequent solution annealing heat treatment, the samples were prepared for mechanical tests (tensile strength and elongation). The tests were performed in the Laboratory for material testing at the Faculty of Mechanical Engineering, University of Tuzla. Results of the static tensile test: tensile strength (TS) and elongation (EL) are given in Table 2. Three tests were done for each alloy in both single and repeated tests, and the average values are shown in the Table 2.

To better analyse the influence of chemical composition on mechanical properties, representative diagrams of the dependence of tensile strength and elongation percentage on chromium content are shown (Figure 1).

Table 2. Results of static tensile test

Alloy	A1 aftersolution annealing	A2 after solution annealing	A3 after solution annealing	A4 after solution annealing
Rm - TS (MPa)	865	761	947	889
A (%) – EL(%)	50.9	42.7	51	42.8

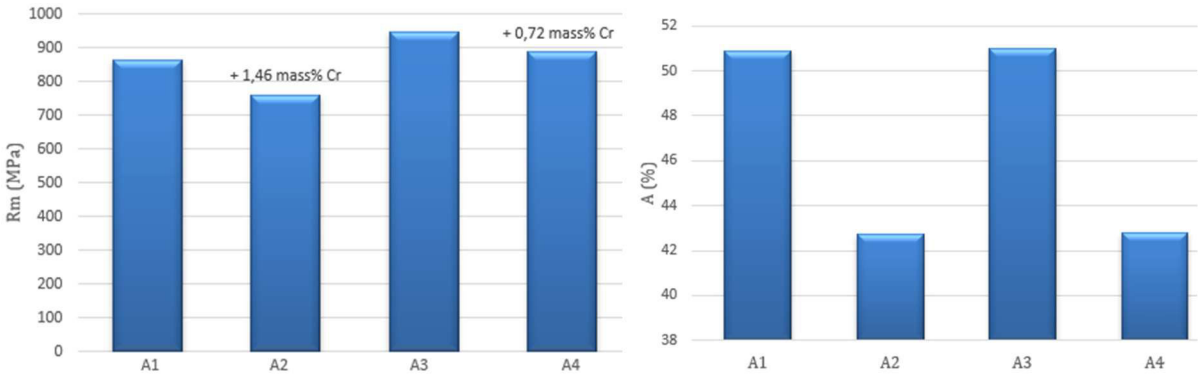

Figure 1. Dependence of tensile strength and elongation percentage on chromium content

Alloys with a higher chromium content have slightly lower tensile strength and significantly lower elongation percentage values. Looking at alloys A1 and A2, according to chemical composition, it is visible that all chemical elements have approximately the same percentage share, and that the biggest difference is in the share of chromium. In alloy A2, the value of chromium is higher by 1.46 mass% compared to alloy A1, Fe-16Cr-8Mn (Mo)-N, which resulted in a drop in the value of tensile strength (TS) by 12% and the EL value by 16,1%. Chromium has a great influence on the reduction of TS and EL. It was also shown for the other two investigated alloys. Alloy A4 contains a higher proportion of chromium by 0.72 mass% compared to alloy A3, Fe-16Cr-

11Mn (Mo)-N, which led to a drop in the TS value by 6.1% and in the EL value by 16%.According to previous extensive studies [1], this claim has also been proven and this paper presents only a part of the research.

2.2. Examination of samples by optical microscopy and SEM

Preparation of samples (grinding, polishing, etching with Vilella's reagent - for high alloy steels and stainless steels, outlines constituents such as carbides, nitrides, sigma phase and delta ferrite.) for light microscopy, as well as the microstructure analysis itself, was done at the Institute for Welding in Tuzla. Three metallographic samples were observed from each alloy. The microstructure of the representative samples is shown in Table 3. After obtaining the microstructure, the content of δ-ferrite and precipitates was assessed using metallographic analysis (ImageJ software - for phase analysis of the microstructure), Table 4.

Table 3. Microstructure of A1, A2, A3 and A4 alloy

A1	A2
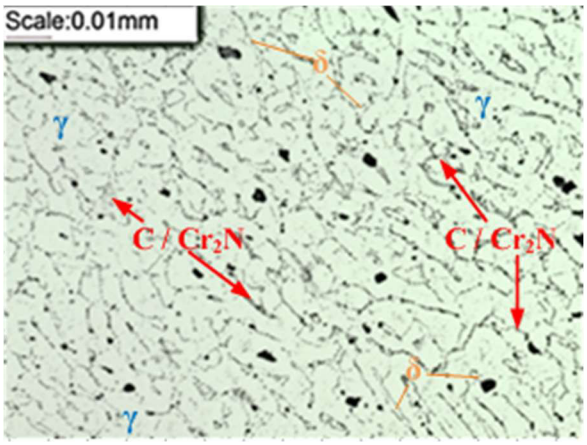	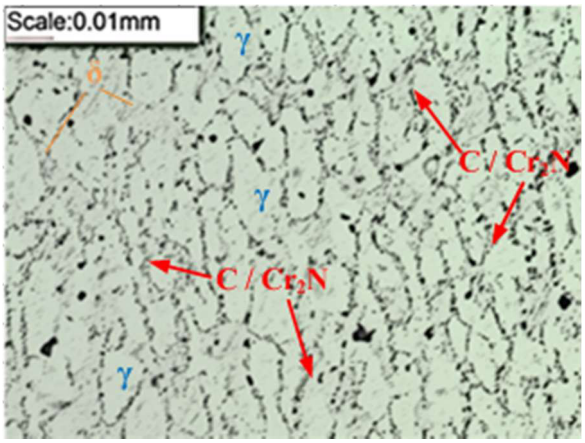
A3	**A4**
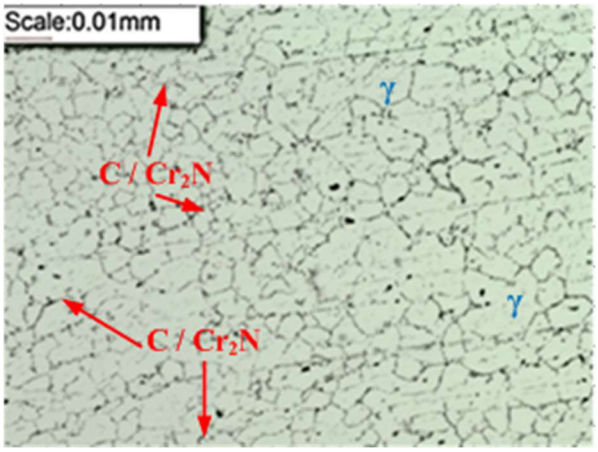	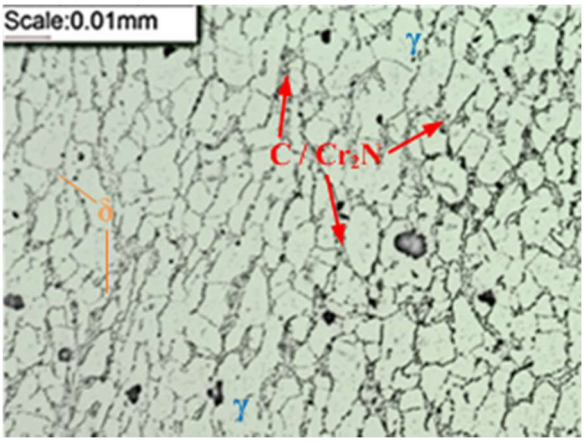

Table 4. Assessment of δ-ferrite and precipitate content (%)

Alloy	A1	A2	A3	A4
Delta Ferrite + Precipitates	9.5	11	8	15

By analysing the microstructures of samples, it was concluded that a two-phase microstructure was formed, austenite and δ-ferrite. Also, in addition to the formation of a two-phase microstructure, it is evident that chromium nitrides were formed in the form of precipitates at the grain boundaries and within the grains, as well as carbides that precipitated at the grain boundaries.

Comparing the chemical analysis and contents of delta ferrite and precipitates, it can be noted that melt A3, which has the lowest content of alphagenic elements (Cr, Si, Mo) has the lowest content of delta ferrite and precipitates and vice versa, melts with a higher share of alphagenic elements have a higher share of delta ferrite and precipitates. In addition to chromium being a big promotor of delta ferrite, it also affects the occurrence of higher content of chromium nitrides.

To precisely determine the chemical compositions, specifically which phases are present in the melts, micro-chemical analysis was done on certain samples in the Laboratory for SEM at the University of Belgrade. Analysis (SEM and EDS) was done on a scanning electron microscope JEOL JSM-6610LV. Results of the analysis for melts A4and A3are shown in Figures 2 and 3, which were formed based on EDS micro-chemical analysis (Tables 5 and 6). These alloys were selected for the observation to clearly show the influence of chromium on the final microstructure, i.e. on the appearance of delta ferrite.

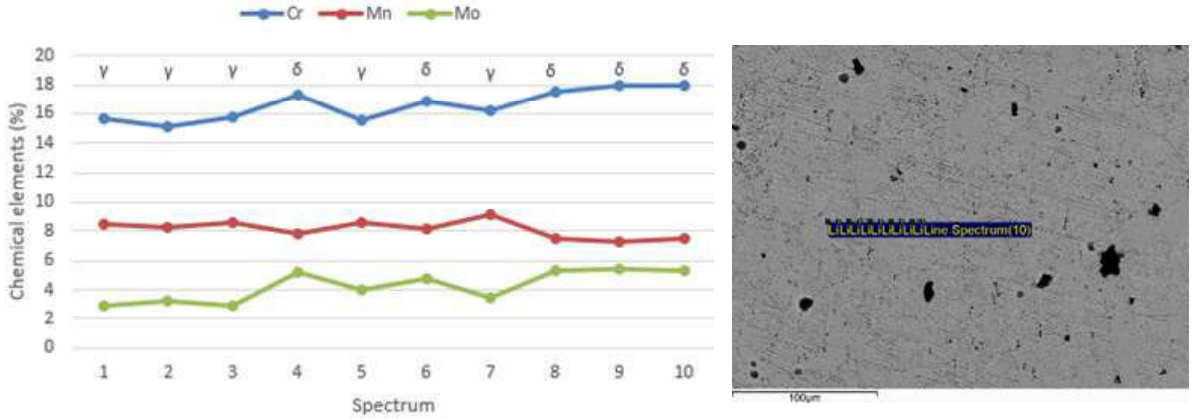

Figure 2. Distribution of elements in delta ferrite and austenite in the alloy A4

Table 5. Results of EDS micro-chemical analysis for alloy A4

Spectrum	Chemical composition (%)				
	Si	Cr	Mn	Fe	Mo
1	/	15.62	8.45	68.53	2.92
2	0.26	15.13	8.24	65.60	3.28
3	0.28	15.75	8.55	67.82	2.95
4	0.28	17.26	7.80	65.83	5.26
5	0.27	15.55	8.60	67.36	4.01
6	0.32	16.90	8.16	66.13	4.78
7	/	16.16	9.15	68.28	3.48
8	0.26	17.56	7.53	66.07	5.31
9	0.31	17.95	7.26	66.37	5.40
10	0.25	17.98	7.54	65.76	5.27

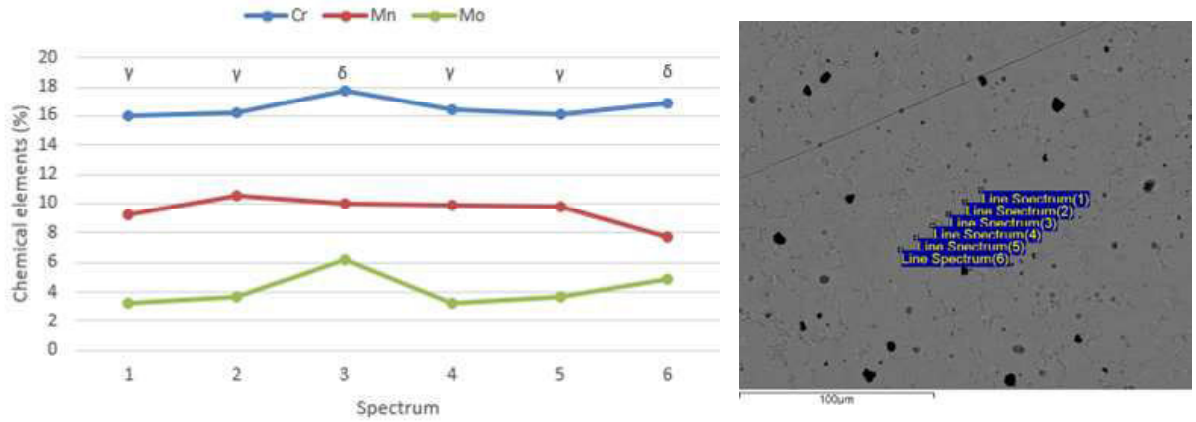

Figure 3. Distribution of elements in delta ferrite and austenite in the alloy A3

Table 6. Results of EDS micro-chemical analysis for alloy A3

Spectrum	Chemical composition (%)				
	Si	Cr	Mn	Fe	Mo
1	/	16.03	9.29	67.34	3.22
2	0.34	16.18	10.55	67.93	3.70
3	0.31	17.69	9.96	65.82	6.22
4	/	16.39	9.88	65.92	3.20
5	/	16.08	9.75	66.09	3.64
6	0.38	16.84	7.69	63.42	4.83

Analysis at the microchemical level confirmed that even after heat treatment, a part of delta ferrite remained that was not completely dissolved, which ultimately reduces the values of mechanical properties, i.e. tensile strength and percentage elongation.

Furthermore, analysing the microstructures, it is clear that not all precipitates have been eliminated. Precipitation of the δ-ferrite in the austenite matrix is possible depending on the chemical composition of steel. Delta ferrite was present even before the solution annealing heat treatment. The very goal of solution annealing is the presence of austenite microstructure at room temperature due to rapid cooling from elevated temperatures.

Applying an annealing temperature of 1100°C led to the decomposition of delta ferrite into carbides, sigma phase and austenite [1, 10]. Since delta ferrite is rich in chromium, the carbides that are excreted are mostly chromium carbides or, depending on the temperature, chromium nitrides can also be separated [1, 7]. A high chromium content increases the solubility for nitrogen and as a consequence, the γ/(γ +Cr_2N) transition is shifted towards lower annealing temperatures [1, 11]. On the other hand, a reduction in chromium results in an increase of the critical temperature for Cr_2N-precipitation [1, 11].These grey clusters are more present in alloys A2 and A4 due to the higher chromium content. The largest content of grey aggregates is found in alloy A2, both due to the highest content of chromium and nitrogen, and due to the lower amount of manganese compared to alloy A4.

It is a proven fact that increasing the manganese content suppresses the formation of chromium nitride [12], which was also confirmed in the analysed alloys. Analysing all the alloys, it is noticeable that even if alloy A2 has the highest proportion of nitrogen, it does not have the highest tensile strength and elongation, because increasing the chromium content requires more nitrogen to form the austenite base, that is, larger amounts of precipitates are formed, while the austenite base is depleted with nitrogen [1,12]. Alloy A3 has the best mechanical properties, because as can be seen from Tables 3 and 4, it has the smallest

proportion of delta ferrite and precipitates, which is visible in the microstructure of this alloy.

3. CONCLUSIONS

The research aimed to determine the effects of chromium in nickel-free austenitic stainless steel Cr-Mn-Mo-N on the microstructure and mechanical properties of this steel. After all the tests were carried out, it is possible to draw the following conclusions:

- A higher content of alphagenic elements affects the production of a larger amount of delta ferrite and precipitates in the formed microstructure of the alloy. To prevent the appearance of delta ferrite, it is necessary to keep the content of the elements that stabilize austenite, manganese and nitrogen close to the upper limit, while the other elements, chromium and molybdenum, should be kept around the middle of the allowed content. In this research, it was shown that a chromium content of 16 mass% is sufficient.
- A series of experiments showed that increasing the chromium content by 1.46 mass% in the Fe-16Cr-8Mn (Mo)-N alloy led to a decrease in the TS value by 12% and in the EL value by 16.1%, while increasing the chromium content by 0.72 mass% in the Fe-16Cr-11Mn (Mo)-N alloy caused a decrease in the TS value by 6.1% and in the EL value by 16%.
- Increasing the content of alphagenic elements, especially chromium, leads to the formation of larger clusters of chromium nitride that directly lower the mechanical properties. Besides that, a higher proportion of chromium ensures a higher content of delta ferrite, which also lowers the values of tensile strength and percentage elongation.

Acknowledgments

The research presented in this paper was financially supported by the Federal Ministry of Education and Science of Bosnia and Herzegovina (Nr. 01-3840-8/23).

Conflicts of Interest

The authors declare no conflict of interest.

4. REFERENCES

[1] J. Halilović, Uticaj parametara nitriranja i naknadne termičke obrade na mikrostrukturu i mehaničke osobine austenitnih nehrđajućih čelika bez nikla, [doctoral dissertation], University of Zuzla, Faculty of mechanical engineering, 2019.

[2] G.V. Gavriljuk, H. Berns, High Nitrogen Steels - Structure, Properties, Manufacture, Applications. Springer-Verlag, Berlin, 1999

[3] J. Pan, C. Karlén, and C. Ulfvin, Electrochemical study of resistance to localized corrosion of stainless steels for biomaterial applications. *J. Electrochem. Soc.*, 147 (2000) 3, pp. 1021-1025

[4] A. F. Padilha, P. R. Rios, Decomposition of Austenite in Austenitic Stainless Steels. *ISIJ*, 42 (2012) 4, pp. 325-337

[5] R. W. K. Honeycombe and H. K. D. H. Bhadeshia, Steels – Microstructure and Properties. Third Edition, University of Cambridge, 2006

[6] Berns H., Alloy development and processing. 7th International Conference on High Nitrogen Steels, Ostend, Belgium, 2004.

[7] J. Halilović, D. Sprečić, E. Nasić, Dž. Kovačević, Effect of solution annealing parameters on microstructure and mechanical properties of nickel free austenitic steels, 16th International Conference on Accomplishments in Mechanical and Industrial Engineering, Banja Luka, 2023.

[8] J. Halilović, S. Butković, E. Nasić, Dž. Kovačević, Microstructure and mechanical properties of nickel free austenitic stainless steels produced by addition of nitrided ferroalloys during melting in induction furnace, TMT 2018, 2018.

[9] L. Hua-Bing, J. Zhou-Hua, High Nitrogen Austenitic Stainless Steels Manufactured by Nitrogen Gas Alloying and Adding Nitrided Ferroalloys, *Journal of Iron and Steel Research*, 14 (2007) 3, pp. 63-68.

[10] A. Gigović-Gekić, H. Avdušinović, A. Hodžić, E. Mandžuka, Effect of Temperature and Time on Decomposition of δ-ferrite in Austenitic Stainless Steel, *Materials and Geoenvironment*, 67 (2020) 2, pp. 65 - 71

[11] P. J. Uggovitzer, R. O. Magdowski, M. Spiedel, Nickel Free High Nitrogen Austenitic Steel. *ISIJ International*, 36 (1996) 7, pp. 901-908.

[12] W. Qingchuan, R. Yibin, Y. Chunfa, Y. Ke, R. D. K. Misra, Residual Ferrite and Relationship Between Composition and Microstructure in High-Nitrogen Austenitic Stainless Steels, *Metallurgical and Materials Transactions A*, 46 (2015) 12, pp. 5537 - 5545

JST&M 6(2024), 22 - 28
DOI: 10.57131/jstm.2024.6.4

Professional paper

EFFECT OF PRECIPITATION HARDENING ON MICROSTRUCTURE OF 17-7 PH STEEL WITH MODIFIED CHEMICAL COMPOSITION

Belma Fakić, Derviš Mujagić, Omer Beganović

University of Zenica, Institute "Kemal Kapetanović"

ABSTRACT

Steel 17-7PH is austenitic-martensitic steel with high strength, hardness, and resistance to creep, and corrosion. It is designed for aerospace components, but can also be used for other applications that require high strength and corrosion resistance, as well as leaf springs for operation at temperatures up to 316 °C. It can be used in a solution-treated or heat-treated state to obtain a wide range of property values. This paperwork shows that modification of the contents of alloying elements with a narrower interval of Cr, Ni, and Al can be obtained from austenitic-martensitic steel 17-7PH which by, a subsequent heat treatment, can have values of mechanical and chemical properties required for components of an automotive engine. Chromium is an alphagenic alloying element that stabilizes the ferrite region, nickel is a gammagenic alloying element that stabilizes austenite and gives these steels good strength and toughness, even at low temperatures and aluminum increases corrosion resistance in low-carbon corrosion-resistant steels Research has determined the most suitable interval of Cr, Ni, and Al, which in combination with the cryogenic heat treatment RH950 at -50 °C gives the mechanical and chemical properties that meet the requirements for steel with standard chemical composition.

Keywords: Heat treatment, mechanical properties, microstructure, precipitation-hardened semi-austenitic stainless steel

Corresponding Author:
Belma Fakić,
University of Zenica, Institute "Kemal Kapetanović" in Zenica
Travnička cesta 7, 72000 Zenica, B&H
Tel.: +387 61 588 883; fax: +387 32 247 980.
E-mail address: belma.fakic@unze.ba

1. INTRODUCTION

Thanks to the complex chemical composition (alloying with aluminum, molybdenum, etc.) and heat treatment, precipitation-hardened steels are a great challenge for metallurgists. Research into different combinations of the chemical composition of materials and heat treatment temperatures provides opportunities for the development of existing and creation of new types of these steels, but also for obtaining high-performance materials with lower production costs and a wider field of application.

2. PRECIPITATION-HARDENED STAINLESS STEELS

Designers of stainless steel products are faced with making tradeoffs between the properties needed for manufacturing and those required for its end use. Precipitation-hardened (PH) stainless steels are iron-chromium-nickel alloys with one or more precipitation-hardening elements such as aluminum, titanium, copper, niobium, and molybdenum. PH stainless steels were developed as a material for the aviation and space industry. But today they are gaining wider commercial importance because they are cost-effective and available in a wide

range of products (bars, wires, forgings, sheets, strips) [1]. These steels are characterized by a unique combination of high strength, toughness, good corrosion resistance, and ease of plastic processing [1].
PH stainless steels are available in one of two conditions – annealed (condition A) or tempered (condition C). The annealed alloys are relatively soft and formable. After forming parts can be age-hardened. Tempered alloys are passed through a rolling mill at room temperature to impart an element of cold work, usually 60 %. From this condition, the alloys can be heat treated to exceptionally high hardness levels and yield strengths in 1200 to 1790 N/mm^2 range. Condition C is the starting point for high-strength parts, but forming must be minimal and simple, with generous radii [2].
PH stainless steels are divided into three groups [1,3]:

- martensitic – 17-4 PH (AISI 630), 15-5 PH, PH 13-8Mo;
- austenitic – A-286 (AISI 600), 17-10 P, HNM;
- semi-austenitic – 17-7PH(AISI 631), PH 15-7Mo, PH 14-8.

The position of PH stainless steel in the Schaeffler-Delong diagram is given in Figure 1.

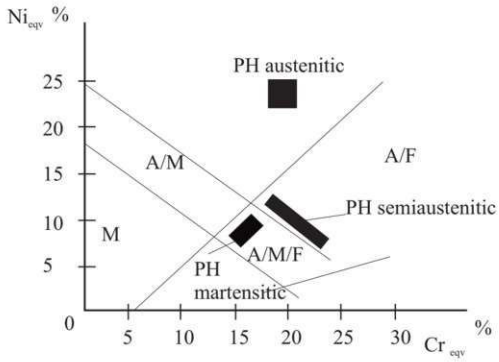

Figure 1. Position of PH steel in the Schaeffler-Delong diagram [3].

3. SEMI-AUSTENITIC PRECIPITATION-HARDENED STAINLESS STEELS

Semi-austenitic stainless steels are precipitation-hardened alloys in which heat treatment can achieve a wide range of required property values. These alloys are used for their combination of high strength, high toughness, and corrosion resistance. Semi-austenitic stainless steels, however, have low fracture toughness in high-strength conditions and a low (subzero) temperature.
The semi-austenitic stainless steels are variants of common austenitic stainless steels with additions of alloying elements such as aluminum and molybdenum. Table 1 lists the approximate composition specification ranges for several common semi-austenitic stainless steels [4].

Table 1. Compositions (wt %) of several common semi-austenitic (precipitation-hardened) stainless steels [4]

Steel		C	Si	Mn	Cr	Ni	Mo	Al
S 17700	17-7PH	max 0.09	max 1.00	max 1.00	16.00-18.00	6.50-7.75	---	0.75-1.50
S 15700	15-7PH	max 0.09	max 1.00	max 1.00	14.00-16.00	6.50-7.75	2.00-3.00	0.75-1.50
S 14800	14-8PH	max 0.05	max 1.00	max 1.00	13.75-15.00	7.75-8.75	2.00-3.00	0.75-1.50
S 35000	AM-350	0.07-0.11	max 0.50	0.50-1.25	16.00-17.00	4.00-5.00	2.50-3.25	---
S 35500	AM-355	0.10-0.15	max 0.50	0.50 - 1.25	15.00-16.00	4.00-5.00	2.50-3.25	---

4. HEAT TREATMENT OF SEMI-AUSTENITIC PH STAINLESS STEELS

Heat treatment of precipitation-hardened (PH) stainless steel is carried out to achieve different levels of mechanical properties related to achieved microstructure. The first step in the heat treatment of PH stainless steels is solution annealing. The aim of solution annealing is to dissolve all secondary phases that may be present in the matrix phase to obtain γ–solid solution. Rapid cooling from the solution annealing temperature suppresses the phase transformation of the high-temperature phase into phases stable at low temperature, i.e. homogeneous compressed solid solution is obtained at room temperature [1,5].

The precipitation-hardened stainless steel can attain high mechanical properties and good resistance [6].

Semi-austenitic precipitation hardened stainless steel 17-7PH is austenitic in the solution annealed state, while after the heat treatment of precipitation strengthening it is martensitic. Precipitation takes place from indirectly achieved martensite. The prefix "semi" means that the austenite in these steels is metastable rather than stable at room temperature [7]. Semi-austenitic steels can contain up to 20% delta ferrite after annealing in their predominantly austenitic microstructure [1].

4.1 Heat treatment of semi-austenitic steel 17-7PH

The influence of the solution annealing temperature on the formation of martensite during quenching is shown in Figure 2. In the case of 17-7PH steel, after quenching at a temperature of 1020 °C, an austenite-ferrite microstructure (60 – 90 % austenite) remains, which enables easier machining. The lower part of the picture shows that by cooling to temperatures of 50 °C and more degrees below zero, the residual austenite turns into martensite. Figure 2 shows that in the case of a higher temperature of solution annealing, the temperature of the beginning of martensite formation is lower. The austenite transformation into martensite is the first stage of strengthening of semi-austenitic stainless steel [8].

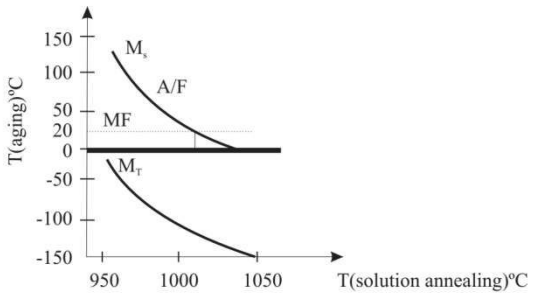

Figure 2. Effect of solution annealing temperature on the martensite formation during quenching [8]

The high strength of precipitation-hardened stainless steel 17-7PH is achieved in three steps: austenite conditioning, cooling below the critical temperature, which can be below zero, transforming austenite into martensite, and precipitation hardening.

Standard heat treatment steps for conditions TH1050 and RH950 are given in Table 2.

Table 2. Heat treatment steps for conditions TH1050 and RH950 [9]

Treatment	State RH950	State TH1050
Solution annealing State A	Austenite conditioning Heating at 955 °C, holding for 10 minutes, cooling at the air to room temperature	Austenite conditioning Heating at 760 °C, holding for 90 minutes, cooling at the air to room temperature
	Transformation Within one hour, start cooling to -75 °C, hold for 8 hours, and heat in air to room temperature	Transformation Within one hour, start cooling to 15±3 °C, hold for at least 30 minutes
	Aging Heating at 510 °C, holding for 90 minutes, cooling at the air to room temperature	Aging Heating at 565 °C, holding for 90 minutes, cooling at the air to room temperature
	Tensile strength after aging	Tensile strength after aging

1450-1650 N/mm^2	1240-1450 N/mm^2

Solution annealing involves heating the material to a temperature at which all elements are dissolved in a solid solution [1]. In 17-7PH steel, by solution annealing at temperatures around 1050 °C, all the carbon goes into solid solution (giving the austenite stability as in type 301 steel). During solution annealing, aluminum dissolves. After cooling, aluminum remains in solution. Since the steel at this stage has an austenitic microstructure, it means that it is relatively soft, ductile and easily formed into the required shape and dimension. Annealing results in the precipitation of $M_{23}C_6$ carbide, which is a deliberate increase in the sensitivity of the alloy. The increase in sensitivity is the consequence of a decrease in the chromium content around the precipitated carbides, which causes an increase in the M_s temperature due to a lower carbon and chromium content in the austenite solution. Depending on the temperature at which the annealing was carried out, the M_s temperature can be controlled so that the transformation to martensite can start at temperatures close to room temperature or at temperatures below zero. The lower level of strength achieved in the TH condition reflects the lower carbon content of the martensite.

4.2 Aging

Aging is a relatively low-temperature heat treatment that hardens the material by precipitation of secondary phases from a supersaturated solid solution [1]. The first stage of hardening of steel 17-7PH is the transformation of austenite into martensite. At solution annealing temperatures, the steel is in the austenitic region. The solubility of carbon in γ-iron is significantly higher than in α-iron. During rapid cooling, γ phase transforms into the phase. Due to the high cooling rate, carbon is unable to leave the BCC lattice (Body Centered Cubic Lattice) of the α phase, which is why the BCC lattice is deformed into a BCT lattice (Body Centered Tetragonal Lattice). This tetragonal α phase is martensite, a supersaturated carbon solid solution in α-Fe, which has greater hardness and strength than austenite. Steel 17-7PH has a low carbon content, so the martensite formed by hardening is soft.

Martensite hardening is the result of the following effects:

- very pronounced solvent hardening,
- high density of dislocations or doubles,
- fewer sliding systems in the BCT lattice compared to the BCC lattice,
- crushing of martensite tiles and
- formation of appropriate precipitates.

4.2.1 State of TH1050

During austenite conditioning at 760 °C, chromium carbides precipitate at grain boundaries or in other high-energy areas, e.g. on slip planes. By reducing the effective content of carbon and chromium in austenite, precipitation leads to transformation during cooling. After treatment at 760 °C, only 0.016 % C remains in the solid solution [1].

Austenite transformation into martensite starts at around 95 °C, and the reaction continues by lowering the temperature and ends by holding for 30 minutes at 15 °C. It is important to note that the cooling from 760 °C to 15 °C should be carried out within one hour, to complete the transformation.

Aging is an additional increase in hardness and strength and is achieved by aging the transformed material by precipitation of secondary phases and additional precipitation of carbides. Hardening during aging reaches a maximum at 510 °C, but is accompanied by minimal ductility. Thus, the heating goes up to 565 °C, where the strength value is slightly lower, but the ratio of strength and ductility values is improved..

4.2.2 State of RH950

After austenite conditioning at 955 °C, 0.034 % of carbon remains in a solid solution. The result of this treatment is an increase in temperature of M_s close to room temperature. Thus, the material conditioned at 955°C retains the austenite microstructure by cooling to room temperature, so it must be transformed with cooling to -75 °C. If the conditioning temperature is higher than 955 °C, martensitic transformation is suppressed,

so cooling to -75 ºC will not lead to complete transformation into martensite.

Austenite transformation after conditioning at 955 ºC, cooling to -75 ºC, and holding for eight hours at this temperature, starts the transformation of austenite into martensite. Most of the transformation occurs during cooling to -75 ºC and the first hour at this temperature.

Aging is an additional increase in hardness and strength and occurs at 510 ºC for one hour. Higher or lower aging temperatures give lower strength, but at higher aging temperatures, better ductility is obtained [1].

5. EXPERIMENTAL PART

The main subject is research on the effect of precipitation hardening on the microstructural characteristics of 17-7 PH stainless steel.

5.1 Chemical analysis

The prescribed chemical composition according to BAS EN 10088-5 standards and the achieved chemical composition of the steel batch are given in Table 3.

Table 3. Chemical composition [1]

Standard/Batch	Chemical composition, wt %							
	C, max	Mn, max	Si, max	P, max	S, max	Cr	Ni	Al
BAS EN 10088-5	0.04	0.52	0.53	0.009	0.023	14.5	7.8	1.53
V1783	0.05	0.55	0.51	0.011	0.029	15.6	7.4	1.18

5.2 Solution annealing

After finished plastic processing, the ϕ 16 mm bars were heat treated as follows:

- heating to a temperature of 1050ºC for 115 minutes,
- heating to a temperature of 1050 ºC for 115 minutes,
- hold to a temperature of 1050 °C for 30 minutes and cooling in the air.

5.3 Precipitation heat treatment

Precipitation hardening of bars was done according to the standard condition TH1050, and condition RH950 was performed by modifying the standard heat treatment as shown in Table 4.

5.4 Mechanical properties

The testing of mechanical properties at room and elevated temperatures was carried out on the Universal hydraulic machine for static tests - AMSLER, in the measurement range from 0 to 200 kN. The literature values of the mechanical properties for the conditions TH1050 and RH950 and the results of the mechanical properties test at room and elevated temperature are given in Table 5.

5.5. Metallography testing

As part of the metallographic tests, an analysis of the microstructure of the samples was carried out on an optical microscope OLYMPUS PMG3. After metallographic preparation (grinding and polishing), samples were etched in reagents for stainless steels.

The best results were shown by the Kalling reagent [10] with composition:

- 100 cm^3 of hydrochloric acid HCl,
- 5 g of copper II chloride $CuCl_2$ and
- 100 cm^3 of ethanol C_2H_5OH.

5.6. Microstructure evaluation

After etching all the samples are ready for microstructure examination. Microstructures are observed using an optical microscope. Figures 3 and 4 show the observed microstructure.

Table 4. Precipitation hardening [1]

Condition	Austenite conditioning	Transformation	Aging
TH1050	Heating up to 760 °C, 70 minutes Holding at 760 °C,	Within one hour, cooling to 15±3 °C, holding 30 minutes	Heating to 565 °C for 50 minutes holding at that temperature for 90 minutes and cooling in air

Condition	Austenite conditioning	Transformation	Aging
	90 minutes		
Modified RH950	Heating up to 955 °C, 90 minutes Holding at 955 °C, 10 minutes	Within one hour, start cooling to - - 50 °C in dry ice holding 8 hours	Heating to room temperature, heating to 510 °C for 45 minutes and holding at that temperature for 60 minutes, and cooling in air

Table 5. Mechanical properties [1]

Literature/Batch	R_m [N/mm^2]		Hardness HV 10
	Room temperature	Elevated temperature 425 °C	
Metals handbook [10]	1170	-	255-361
AK Steel bulletin [11]	-	986	-
V1783 State TH1050	1419	923	437
Metals handbook [10]	1378	-	438
AK Steel bulletin [11]	-	1103	-
V1783 State RH950	1562	1100	541

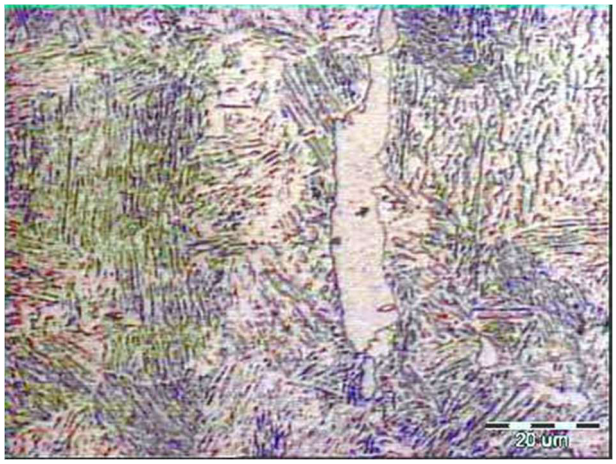

Kalling x750
Longitudinal section

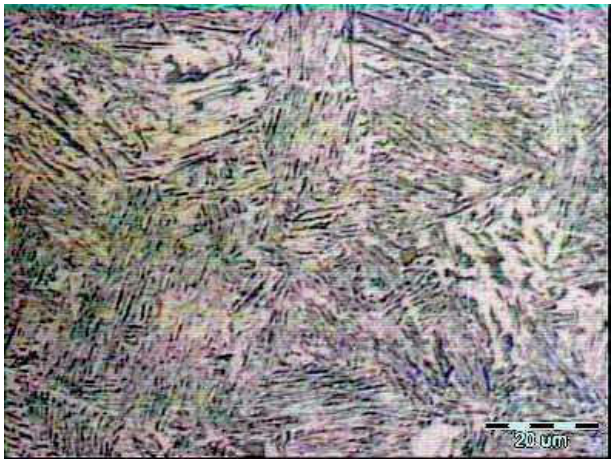

Kalling x750
Cross section

Figure 3. State TH1050, batch V1783; martensite, austenite and delta ferrite [1]

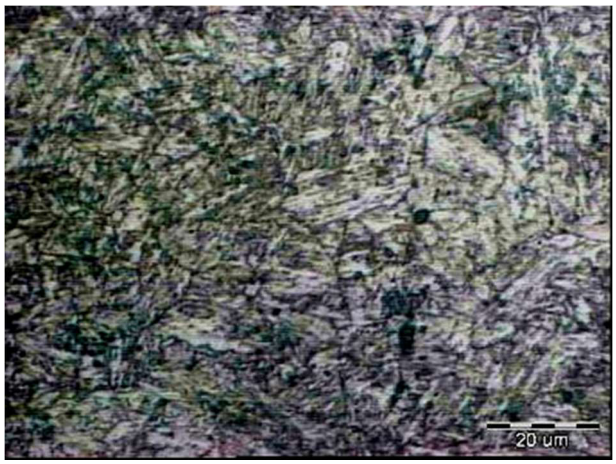

Kalling x750
Longitudinal section

Kalling x750
Cross section

Figure 4. State RH950, batch V1783; martensite, austenite, and delta ferrite [1]

6. CONCLUSIONS

The research aimed to determine the effects of precipitation hardening on the microstructure of 17-7PH steel with modified chemical composition. Steel 17-7PH with a modified chemical composition, with a lower chromium content and a narrower range of nickel and aluminum content, shows higher values of mechanical and chemical properties in the RH950 state compared to the TH1050 state. The modified heat treatment of precipitation hardening RH950 carried out at -50 °C achieved very good mechanical properties of steel with modified chemical composition. The amount of delta ferrite in the TH1050 state is about 5 % and retained austenite is about 1 5%. The amount of delta ferrite in the RH950 state is less than 5% and retained austenite about 19 %.

Conflicts of Interest

The authors declare no conflict of interest.

7. REFERENCES

[1] B. Fakić, *Modifikacija sadržaja kroma, nikla i aluminija u precipitaciono ojačanom čeliku 17-7PH namijenjenog za proizvodnju komponenti automobilskih motora*, [doktorska disertacija], Univerzitet u Zenici, Fakultet za metalurgiju i materijale, Zenica, 2015.

[2] https://www.ulbrich.com/blog/precipitation-hardening-stainless-steel-alloys-guide/, available february 2024.

[3] P. Hedström**,** *Deformation induced martensitic transformation of metastable stainless steel AISI 301*, Luleå University of Technology Department of Applied Physics and Mechanical Engineering Division of Engineering, Sweden, 2005

[4] https://www.totalmateria.com/page.aspx?ID=CheckArticle&site=kts&NM=445, available december 2023.

[5] H. Šuman, *Metalografija*, Univerzitet u Beogradu, Zavod za izdavanje udžbenika SR Srbije, Beograd, 1962.

[6] https://www.fushunspecialsteel.com/precipitation-hardened-stainless-steels-heat-treatment/, available January 2024.

[7] M. Novosel, Dragomir Krumes, *Posebni čelici*, Slavonski Brod, 1998.

[8] M. F. McGuire, *Stainless Steels for Design Engineers,* ASM International, Materials Park, Ohio 44073-0002, 2008

[9] J. R. Davis, *Alloy Digest Sourcebook: Stainless Steels*, ASM International, 2000

[10] Metals Handbook, *Metallography and microstructure*, Vol. 9., ASM International, 9th edition, 1992.

[11] https://www.aksteel.nl/files/downloads/ak_steel_armco%C2%AE_17-7_ph%C2%AE_product_data_bulletin_-feb__2019-_90.pdf, available January 2013.

JST&M 6(2024), 29 - 34
DOI: 10.57131/jstm.2024.6.5

Professional paper

THE INFLUENCE OF MANGANESE ON THE TENSILE STRENGTH OF HIGH CARBON STEEL C66D

Aida Imamović[1], Omer Kablar[2], Mirsada Oruč[1], Vedina Purić-Selimović[2], Lamija Sušić[1]

[1] University of Zenica, Faculty of Engineering and Natural Science, [2] ArcelorMittal d.o.o. Zenica;

ABSTRACT

Modern steel production cannot be imagined without manganese, because almost all steels contain manganese.
In this paper, we present the impact of manganese on the tensile strength values of high-carbon steel. This paper presents an improvement in the quality of wire rolling with control of manganese content in steel and the value of C-equivalent, in industrial conditions, which is of particular importance in the production of this quality of steel.
For the presented quality of rolled wire made of high-carbon steel, it is possible to control the C-equivalent in high-carbon steel to achieve values for tensile strength in exceptionally narrow tolerances of 1000 ± 30 MPa.

Keywords: high carbon steel, manganese influence, tensile strength, C-equivalent

Corresponding Author:
Aida Imamović
Affiliation:
University of Zenica, Faculty of Engineering and Natural Science
Travnička cesta 1, Zenica 72 000, Bosnia and Herzegovina
Tel.: +387 32 401 831; fax: +387 32 406 903
E-mail address: aida.imamovic@unze.ba

1. INTRODUCTION

Carbon steel or non-alloy steel is of ordinary quality and is classified mainly according to mechanical properties. It is used for lightly loaded parts of machines, devices, vehicles, or for bars and grates. Unalloyed or carbon steels, which, depending on the proportion of harmful phosphorus and sulfur impurities (i.e. purity), can be of ordinary quality with a maximum of 0.050% P and S individually, high-quality with a maximum of 0.045% P and S individually, and noble with a maximum up to 0.035% P and S individually. Carbon steels usually have a content of 0.05 to 1.35% C. To the carbon content, structural steels are further divided into low carbon (up to 0.20 %C), medium carbon (0.20 to 0.50 %C), and high carbon (more than 0.50 %C) [1].

Carbon steels are mainly divided into low-carbon, medium-carbon, and high-carbon steels according to EN 10020 [1]:

- ***Low-carbon steels*** have mainly ferritic microstructure, and their properties are close to pure iron, which is reflected in the possibilities of their welding. Their main disadvantage is the inability to achieve high hardness by hardening. Low-carbon steels have a carbon content of 0.05% to 0.20%.
- ***Medium carbon steels*** have a mixed, pearlitic-ferritic structure. In contrast to low-carbon steels, they have higher strength and hardness, as well as lower toughness and elongation. Medium carbon steels (0.20% - 0.50% of carbon) are used mainly in the normalized state.

- ***High-carbon steels*** have a perlite-cementite structure, which is the main cause of increased hardness and reduced toughness and elongation. They are widely used in the manufacture of tools, because of excellent hardenability, but reduced elongation. High-carbon steels have a carbon content above 0.5%. It has the highest hardness and toughness of carbon steels and the lowest ductility.

2. INFLUENCE OF MANGANESE ON STEEL QUALITY

Modern steel production can not be imagined without manganese, because almost all steels contain manganese. In steel production, manganese is added as a ferroalloy to molten steel, thus achieving several beneficial effects. Manganese acts as a deoxidizer and desulfurizer and binds oxygen and sulphur. In addition, the presence of manganese in steel greatly increases the hardness of steel and wear resistance. Due to this, almost all steels contain manganese within certain limits, most often from 0.3% to 1.5%.

Figure 1 shows the positive effect of manganese and carbon content on the tensile strength of hot-rolled steels. Increasing the manganese content increases the tensile strength of rolled products and is especially effective when the upper limit of manganese is allowed. By reducing the manganese content below 1%, the tensile strength decreases significantly, as shown in Figure 1 [2,3].

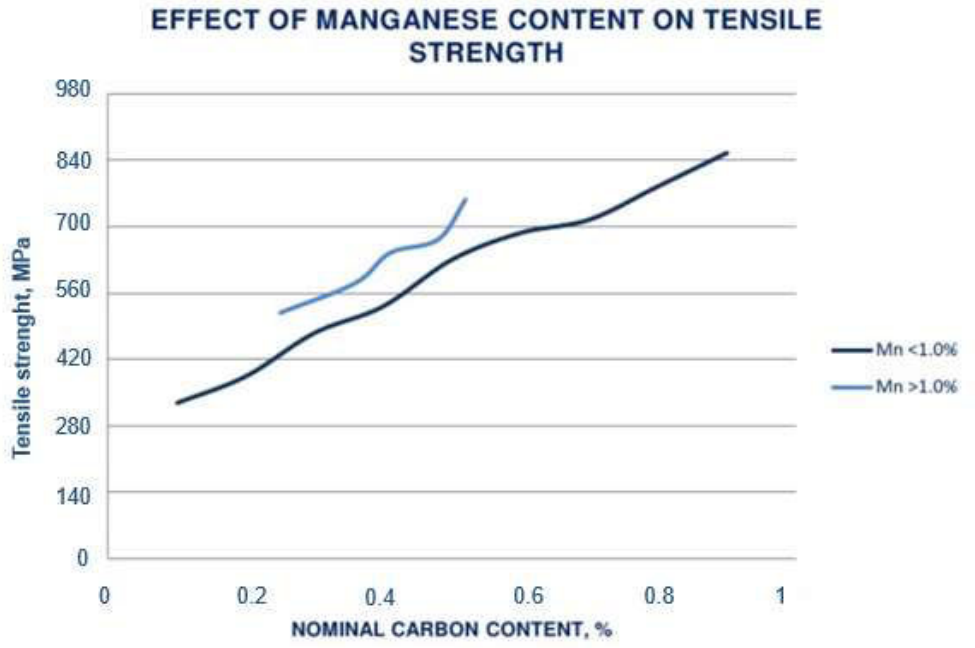

Figure 1. Influence of manganese on tensile strength [3]

The effect of manganese on improving the mechanical properties of steel also depends on the carbon content. Manganese also reduces the critical cooling rate during solidification by shifting the austenite conversion temperature to lower temperatures, thus increasing the hardness of the steel. Manganese also reduces the critical cooling rate during solidification by shifting the austenite transformation temperature to lower temperatures. Its effect on hardness is greater than other alloying elements. Manganese, as a gamma element, expands the austenitic area but also stimulates the formation of coarse grains and the appearance of brittleness.

Both carbon and manganese have been found to have a significant effect on tensile strength. Carbon equivalent (C_{eq}) is an important tool for determining different properties (prediction of hardness, weldability, and microstructure) of an alloy when more elements than carbon are used as an alloying element. C_{eq} calculation is used in welding, heat treatment, and casting

processes. Carbon equivalent (C_{eq}) is used in welding to define the weldability of steel and to know how different alloying elements affect the hardness and microstructure of the material to be welded. As C_{eq} values increase, the weldability of the material decreases. Low carbon equivalent materials offer excellent weldability with minimal precautions [3, 4].

For special shipbuilding and other high-strength steels with a carbon content over 0.18%, C_{eq} can be calculated:

$$C_{eq} = \%C + \frac{(\%Mn + \%Si)}{6} + \frac{(\%Cr + \%Mo + \%V)}{5} + \frac{(\%Cu + \%Ni)}{15} \quad (1)$$

Depending on the amount of carbon equivalent (C_{eq}) obtained, weldability is estimated [5]:

$C_{eq} < 0.25 \rightarrow$ good weldability
$0.25 < C_{eq} \leq 0.35 \rightarrow$ satisfactory weldability
$0.35 < C_{eq} \leq 0.45 \rightarrow$ limited weldability
$C_{eq} > 0.45 \rightarrow$ very poor weldability

3. PRACTICAL WORK

Steel marked C66D is a high-carbon steel with chemical composition according to standard EN ISO 16120 which is used for various purposes and most often for the production of wire intended for drawing. The main characteristic in the industrial production of this steel is the achievement of the requested value of tensile strength. The values of tensile strength were determined in the ArcelorMittal Zenica laboratories according to the BAS EN ISO 6892-1:2017 standard and according to the customer's request.

Table 1. Characteristics of C66D steel according to standard EN ISO 16120 [2]

Element	C	Mn	Si	P	S	Tensile strength R_m (N/mm^2)
mass. [%]	0.63-0.68	0.60-0.90	0.10-0.30	≤ 0.030	≤ 0.030	1000

This type of steel, with manganese in the range of 0.60-0.90, is used for the production of 5.5 mm wire in a coil for the following use: production of reinforcing mesh, cold drawing, ribbing of wire, springs other steel products for general use.

Continuously cast billets with dimensions of 120x120x12000 mm were used for the production of rolled wire with a diameter of ϕ5.5 mm from steel C66D, the chemical composition of which corresponds to the specified steel according to the EN standard.

Billets are first heated in a walking hearth furnace to rolling temperature 1160°C. The total number of rolling mill stands that rolling piece passed to reach desire diameter 5.5 mm is 25th. To reach mechanical properties according to standard the very important procedure is the thermical treatment STELMOR process.

Thermal treatment performed using the STELMOR process includes:

- Water cooling with two water boxes by adjustment of the valves which supply water to the eater cooling zones. Different adjustment may be required to obtain the same laying temperatures for different wire dimensions. After water cooling, the temperature of the wire for grade C66D is 830 ± 10 °C;
- Cooling with four air fans and with speed adjustment of stelmor conveyor. The conveyor speed is selected to provide appropriate spacing between wire rings on conveyor. And air nozzles are design to supply more cooling at the side of conveyor than at the center in purpose uniformity of properties at all position on the conveyor.

STELMOR process has the role of responding to the requirements of microstructure and mechanical properties by controlled cooling. After cooling with water in two water boxes, the wire is further transport to the STELMOR conveyor where the second phase of cooling begins and that cooling via air fans. After that, coils of wire are formed and thus the cooling process is completed [6]. Cooling conditions

on the conveyor must be set so as to achieve the highest possible cooling speed, which is achieved by establishing the so-called "open ring in the ring" in combination with a sufficient number of high capacity cooling fans, Figure 2.

Figure 2. Air Cooling process at STELMOR

The goal of the STELMOR process is to achieve the highest possible cooling rate, as well as to control the rate of transformation of austenite into ferrite-perlite because by increasing the cooling rate, smaller ferrite grains are obtained and pearlite lamellas become thinner. In that way, a higher degree of cold plastic deformation is enabled until the appearance of fracture.

Because C and Mn contents have a significant effect on tensile strength, therefore, care must be taken about the carbon equivalent C_{eq}. In this case, for C66D steel, C_{eq} was calculated using the following equation [5]:

$$C_{eq} = \%C + \frac{\%Mn}{6} + \frac{\%Cr + \%Mo + \%V}{5} + \frac{\%Cu + \%Ni}{15} \quad (2)$$

In the practical part, 6 samples of C66D steel billets were analyzed, in which the Mn content and the calculated C_{eq} based on the previous equation and are presented in Table 2 [7]:

The value of C-equivalent increases with a higher manganese content and should take into account the mechanical properties of steel, Figure 3.

Table 2. Mn, $C_{eq,}$ and tensile strength of produced C66D steel billets

Sample	1	2	3	4	5	6
Mn	0.66	0.67	0.68	0.68	0.69	0.71
C_{eq}	0.769	0.774	0.791	0.787	0.781	0.820
R_m, MPa	959	969	1050	1009	1005	1059

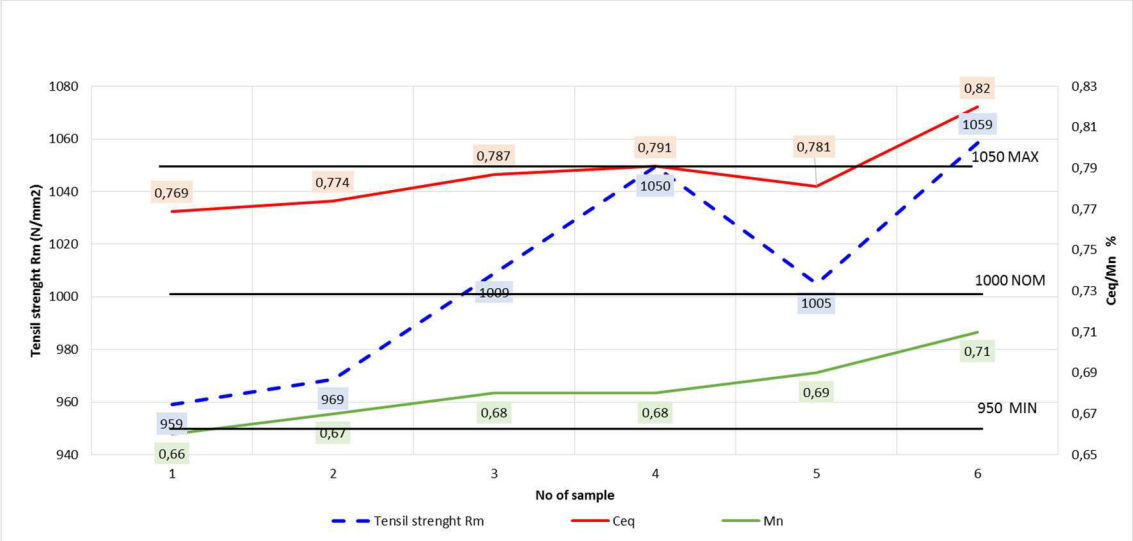

Figure 3. Mn content, C_{eq} value, and tensile strength values of C66D steel

It can be seen from Figure 3 that with a C_{eq} greater than 0.78, tensile strength values of at least 1000 MPa can be achieved with certainty. This value corresponds to a percentage of manganese of 0.68% and carbon equivalent C_{eq} of 0.787. It can be concluded that Mn as an element has a positive effect on tensile strength, which could be seen in melt No. 3 where the tensile strength had the highest value to other melts 1059 MPa, and where the Mn content was also the highest.

By controlling the manganese content, with the same production conditions, i.e. rolling, it is possible to control the tensile strength values of the rolled wire.

For the presented quality of rolled wire made of high carbon steel, it is possible with the current improved technology in ArcelorMittal Zenica with control of C_{eq} value to achieve values for tensile strength (R_m) in tolerance of 1000 ± 30 MPa.

4. CONCLUSION

- With the same parameters of the Stelmor process, the tensile strength for different values of Mn and thus C_{eq} was different.
- Based on the conducted research, it can be concluded that Mn as an element has a positive effect on tensile strength [8].
- In order to achieve higher tensile strength, it is best to limit the Mn content from 0.68% to 0.69%.
- Carbon increases tensile strength as well as manganese. These elements directly affect the value of C_{eq}.
- It can be concluded that the C_{eq} should be kept in the range from 0.78 % to 0.82%.
- Improving the rolling quality of C66D steel wire and controlled values for C_{eq} has contributed to the fact that values for tensile strength can be achieved in a tolerance of 1000 ± 30 MPa.

Conflict of interest

The authors declare no conflict of interest.

5. REFERENCES

[1] M. Oruč, F. Begovac, I. Vitez, R. Sunulahpašić, *Čelik i čelični liv, podjela i označavanje*, Fakultet za metalurgiju i materijale, Univerzitet u Zenici, 2008.

[2] https://www.industrialheating.com/articles/89322-the-influence-of-manganese-in-steel [entery: january 2023]

[3] https://www.slideshare.net/ElementMaterials/element-presentation-on-carbon-and-low-alloy-steels [entery: january 2023]

[4] Carbon equivalent for steel, low alloy, C-Mn steel and cast ...Proinstal

[5] https://proinstal.hr › ekvivalent-uglj. [entery: january 2023]

[6] T. Kostadin, *Čelici i željezni ljevovi, Materijali II*, Veleučilište u Karlovcu, 2017.

[7] Tehničko-tehnološka dokumentacija kompanije ArcelorMittal Zenica d.o.o. (2020-2021)

[8] Š. Žuna, *Doprinos istraživanju uticaja variranja hemijskog sastava konti livenih gredica iz*

konstrukcionih čelika i čelika za vučenje žice na kvalitet toplovaljane i vučene žice, [doktorska disertacija], Univerzitet u Zenici, Fakultet za metalurgiju i materijale, 2016.

[9] A. Imamović, O. Kablar, M. Oruč, V. Purić, A. Gigović-Gekić, Poboljšanje kvaliteta valjane žice od visokougljeničnog čelika sa kontrolom vrijednosti C-ekvivalenta, 12th Research/Expert Conference with International Participations "QUALITY 2021", Neum, B&H, June 17 – 19, 2021.